MESMER: An open-source **M**aster **E**quation **S**olver for **M**ulti-**E**nergy well **R**eactions

David R. Glowacki,[a]* Chi-Hsiu Liang, Christopher Morley, Michael J. Pilling, and Struan H. Robertson*†

School of Chemistry, University of Leeds, Leeds LS2 9JT, UK

[a]School of Chemistry, University of Bristol, Bristol BS8 1TS, UK

†Accelrys Ltd., 334 Cambridge Science Park, Cambridge, CB4 0WN, UK

*drglowacki@gmail.com; struanr@accelrys.com

Abstract

The most commonly used theoretical models for describing chemical kinetics are accurate in two limits. When relaxation is fast with respect to reaction timescales, thermal transition state theory (TST) is the theoretical tool of choice. In the limit of slow relaxation, an energy resolved description like RRKM theory is more appropriate. For intermediate relaxation regimes, where much of the chemistry in nature occurs, theoretical approaches are somewhat less well established. However, in recent years master equation approaches have been successfully used to analyze and predict non-equilibrium chemical kinetics across a range of intermediate relaxation regimes spanning atmospheric, combustion, and (very recently) solution phase organic chemistry. In this paper, we describe MESMER, a user-friendly, object-oriented, open-source code designed to facilitate kinetic simulations over multi-well molecular energy topologies where energy transfer with an external bath impacts phenomenological kinetics. MESMER offers users a range of user options specified via keywords, and also includes some unique statistical mechanics approaches like contracted basis set methods and non-adiabatic RRKM theory for modelling spin-hopping. It is our hope that the design principles implemented in MESMER will facilitate its development and usage by workers across a range of fields concerned with chemical kinetics. As accurate thermodynamics data becomes more widely available, electronic structure theory is increasingly reliable, and our fundamental understanding of energy transfer improves, we envision that tools like MESMER will eventually enable routine and reliable prediction of non-equilibrium kinetics in arbitrary systems.

Introduction

The treatment of kinetic rate coefficients in a range of physical, environmental, industrial, astrophysical, and biological systems is largely based on equilibrium statistical mechanics – i.e., on Gibbs energies. In this regime, thermal relaxation timescales are much faster than kinetic timescales, and canonical transition state theory (CTST) combined with accurate molecular energies offers a reliable way to calculate rate coefficients.[1] However, a number of chemical reactions occur with non-equilibrium (i.e., non-Boltzmann) energy distributions, giving rise to phenomenological kinetics that cannot be accurately described using the machinery of equilibrium thermodynamics. In such regimes, free energy descriptions are of limited value, often because the timescales for thermalization are competitive with kinetic timescales. One successful theoretical approach for treating this competition uses a stochastic energy grained master equation (EGME). The EGME typically involves the calculation of energy resolved rate coefficients using microcanonical transition state theory (μTST) and collisional energy transfer models. These are combined to construct a model describing phenomenological rate coefficients that arise from competition between reaction and thermalization of non-equilibrium ensembles. This approach has proven successful in the gas phase – particularly in combustion chemistry and atmospheric chemistry. Recently, the EGME has even been extended to resolve the microscopic details of non-equilibrium kinetics occurring in solution phase synthetic organic chemistry.[2,3]

Generally speaking, the phenomenological quantities of particular interest in kinetic modelling – e.g., for use in process models – include rate coefficients, time dependent species profiles, product yields and reaction channel branching ratios. Each of these typically show a complex dependence on pressure and temperature. One reason for the utility of the EGME is that many industrial and environmental processes take place at temperatures and/or pressures that are difficult to access in experimental studies of elementary reactions. The EGME is a practical theoretical tool that allows one to optimize kinetic parameters at experimentally accessible conditions, and subsequently predict kinetics in experimentally inaccessible regimes. For example, experimental kinetics measurements of chemical reactions important in combustion are performed at temperatures and pressures that are typically much lower than those of real combustion systems. Similarly, experimental measurements of atmospheric systems typically occur at pressures much lower than those relevant in the atmosphere. In

such cases, the EGME provides a quantitative means of extrapolating results obtained under laboratory conditions to "realistic" conditions. A similar situation arises not only in combustion and atmospheric chemistry, but also for interstellar chemistry and industrial chemistry. In principle the EGME – in conjunction with μTST, scattering theory, and *ab intio* calculations of a reactive system's potential energy surface (PES) – is capable of providing a first principles estimate of rate coefficients as a function of temperature and pressure.[4-15]

In this paper, we introduce MESMER, a **M**aster **E**quation **S**olver for **M**ulti-**E**nergy well **R**eactions. MESMER is a recently developed cross-platform, open-source software project (see http://sourceforge.net/projects/mesmer/) which uses matrix techniques to formulate and solve the EGME for unimolecular systems composed of an arbitrary number of wells, transition states, sinks, and reactants. It offers a flexible approach to EGME treatments of complex reactive systems and provides a complementary approach to stochastic simulation programs such as Multiwell which utilize kinetic Monte-Carlo approaches.[16,17] In developing MESMER, we have also attempted to incorporate various facilities that make it easy to use the EGME to directly interpret experimental observables. There are two principal design goals that we have emphasized while writing MESMER. First, we use standard, off-the-shelf technologies, so that the code may be readily maintained and extended. For example, MESMER development has been facilitated by using the Microsoft Visual Studio and Xcode integrated development environments (IDEs), XML data representation for the input stream, and Firefox as a graphical user interface (GUI) to aid in constructing input files and interpreting output files. Current developments are underway to increase compatibility between MESMER and other open source projects as OpenBabel. Second, we have used open source C++ to write structured, object-oriented, cross-platform code with the intent that it will be easy to maintain and extend by future developers. Where possible, we have emphasized plug-in classes to accommodate future developments in several different parts of the code – e.g. partition function treatments, collisional energy transfer models, calculation of microcanonical rate coefficients, and fitting of experimental data.

This paper is structured as follows: in section one we present an overview of the theory of master equations (ME) as applied to gas phase reactions. In section two we discuss in further detail some of the design principles we have adopted in developing MESMER. Section three gives a more detailed discussion of some of MESMER's features, with particular attention to those features unique to MESMER. In section four, we discuss several published examples where we have applied MESMER. Concluding remarks and an outlook are given in section five.

1. The Energy Grained Master Equation: Theory

The form of the EGME discussed in this work is the one-dimensional ME, wherein the total rovibrational energy of the system, *E*, is the independent variable. Indeed, a more thorough treatment would not only consider the time dependent evolution of the system with respect to the total energy, *E*, but also the angular momentum, *J,* as both of are constants of motion.[18] However, two-dimensional ME treatments (i.e., in terms of *E* and *J*) are restricted in their application, given the difficulty of describing the transition probabilities wherein both *E* and *J* are coupled. Presently, 2D approaches may only be used to solve the ME in the collisionless limit,[12,13] or for a system that has a single potential well.[19] Thus, the bulk of ME modelling on systems relevant to atmospheric and combustion chemistry is restricted to a *J* averaged 1D ME,[20,21] for which MESMER has been designed. In general, the 1D ME gives reliable results and consequently it has been adopted by a number of workers. Part of the reason for this is because the errors in molecular properties (e.g., energies and frequencies) and experimental measurements (e.g., of rate coefficients or product yields) tend to have more of an impact on ME results than those errors which are introduced by neglecting *J*.

Scheme 1 shows stationary points on a PES for a typical gas phase unimolecular system. The initial reaction is a bimolecular association, and it is followed by a sequence of unimolecular reactions involving two potential energy wells (local minima). Each well represents a (meta-) stable species that can, in principle, be isolated. Wells are connected by unimolecular transition states (TS) and a species in one well may be converted to another by passing through the TS that connects the wells. In many systems, there is an energy barrier to inter-conversion of species, and the TS corresponds to a first-order saddle point on the molecular PES. Thus, to convert from one species to another, the reactant must be activated – i.e., energy must be supplied to overcome the barrier separating the wells. Typically, energy is supplied to the system through interactions with a thermal bath. In the gas phase, such energy transfer typically occurs through collisions with bath gas molecules. Some of the collisions are activating (i.e., result in a net *increase* in system energy) and some are deactivating (i.e., result in a net *decrease* in system energy), with the relative rate of each type of collision constrained to obey detailed balance. Since collision events and the amount of energy transferred are random quantities, the energy transfer process can be regarded as a random walk, and treated using techniques from stochastic process theory.[8,9]

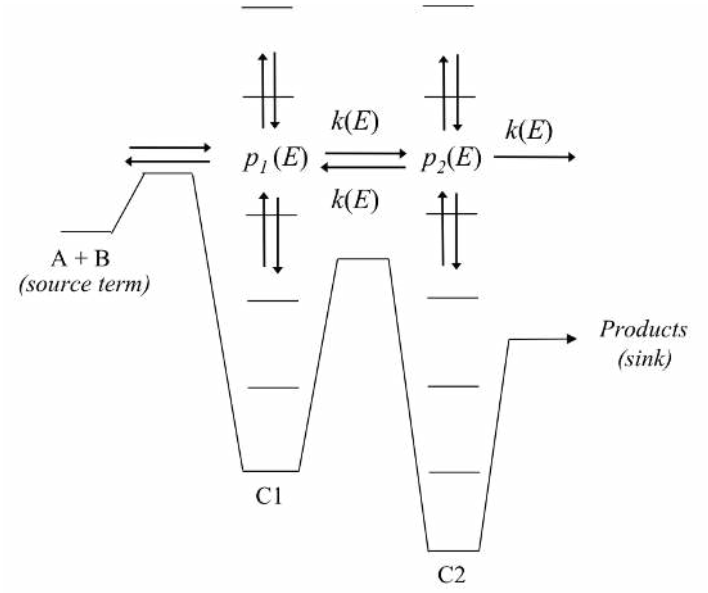

Scheme 1. Representation of the Energy Grained Master Equation model for an association reaction (i.e., source term) with two wells, C_1 and C_2 and an irreversible product channel

The aim of the EGME is to provide a macroscopic kinetic description of a reaction system, such as that shown in Scheme 1, in terms of the behaviour of each of the isomers at an energy resolved (or microcanonical) level. At those energies which are typically significant for describing non-equilibrium kinetics, the number of states in polyatomic molecules tends to be very large, and describing the time evolution of every individual state represents an impossibly expensive computational challenge. The EGME circumvents this problem by bundling together rovibrational states of similar energies into 'grains', and then describing the time evolution between these energy grains, which generally span no more than a few kJ mol^{-1}. The formulation of the EGME in terms of grains essentially corresponds to expanding the solutions in a basis of delta functions whose origins lie at the centre of each grain.

Letting subscript m denote the index of a particular isomer on a reactive PES (e.g., for Scheme 1 where there are two isomers, $m \in 1,2$) and letting E denote the energy of a particular grain, the rovibrational population density within a particular energy grain, $p_m(E)$, may be described by a differential rate equation that accounts for collisional energy transfer within each isomer as well reactive processes that both increase and decrease the grain population:

$$\frac{dp_m(E)}{dt} = \omega \int_{E_{0m}}^{\infty} P(E \mid E')p_m(E')dE' - \omega p_m(E) + \sum_{n \neq m}^{M} k_{mn}(E)p_n(E) - \sum_{n \neq m}^{M} k_{nm}(E)p_m(E) - k_{Sm}(E)p_m(E) + K_{Rm}^{eq} k_{Rm}(E) \frac{\rho_m(E)e^{-\beta E}}{Q_m(\beta)} n_A p_B - k_{Rm}(E)p_m(E) \quad (1)$$

The right hand side (RHS) of Eq (1) has seven terms. Three are positive, corresponding to population flux *into* $p_m(E)$, and four are negative, corresponding to population flux *out of* $p_m(E)$. The first term on the RHS of Eq. (1) describes population gain in $p_m(E)$ – i.e., isomer C_m at energy E – via collisional energy transfer from other energy grains in that isomer. ω is the Lennard-Jones collision frequency, and $P(E|E')$ is the probability that collision with bath gas will result in a transition from a grain with energy E' to a grain with energy E. The second term represents population loss from grain $p_m(E)$ via collisional energy transfer. The third term describes reversible population gain into grain $p_m(E)$ by reactions that transfer population from isomer n to isomer m at a particular energy E ($k_{mn}(E)$ is the microcanonical rate constant for population transfer from grains in isomer n to grains in isomer m). The fourth term describes reversible population loss from $p_m(E)$ via reactions that transfer population from grains in isomer m to the other possible isomers, denoted by index n ($k_{nm}(E)$ are the microcanonical rate coefficients for population transfer from isomer m to isomer n at energy E). The fifth term describes irreversible population loss from $p_m(E)$ via reactions that transfer population from isomer m to products S with microcanonical rate coefficient $k_{Sm}(E)$. The inclusion of such irreversible loss terms introduces an infinite sink approximation, and consequently requires careful consideration when implemented in Eq. (1).[10,22] In general, infinite sink approximations are reasonable in two different scenarios: (i) for unimolecular dissociation processes, so long as re-association timescales are much longer than the phenomenological kinetic timescales under consideration, which is often the case under a range of conditions, e.g. where the concentration of one of the co-reactants in the product set S is negligible; and (ii) for unimolecular isomerizations with an exceptionally large reverse barrier, where the magnitude of the backward rate coefficient, $k_{mn}(E)$, is negligible compared to the forward rate coefficient, $k_{nm}(E)$.

The final two terms in Eq. (1) pertain to the so-called bimolecular source term, and

apply only to those isomers that are populated via bimolecular association reactions (e.g., well C1 in Scheme 1). Assuming (i) that the bimolecular reactants, A and B, are maintained in a Boltzmann distribution on the phenomenological timescale of interest, and (ii) that reactant A is in significant excess compared to reactant B (i.e., [A] >> [B]), and a pseudo-first order kinetics approximation is therefore appropriate, then the sixth and seventh terms respectively describe population gain in $p_m(E)$ from association of reactants A and B (together denoted as R), and population loss from $p_m(E)$ via re-dissociation to reactants. $k_{Rm}(E)$ represents the rate constant at which $p_m(E)$ re-dissociates to give the bimolecular reactants, R, and K_{Rm}^{eq} is the equilibrium constant between isomer m and the reactants. $Q_m(\beta) = \int dE \rho_m(E) e^{-\beta E}$, which is the rovibrational partition function for the molecular species corresponding to isomer m, n_A is the number density of reactant A, and p_B is the population in reactant B.[9,13]

Eq. (1) as written does not represent a closed system of differential equations because p_B is unspecified. In the cases where a bimolecular association reaction is to be included in a reaction network (e.g., in Scheme 1) then an additional differential equation must be included to describe the time dependence of p_B:

$$\frac{dp_B}{dt} = \sum_{m=1}^{M} \int_{E_{0i}}^{\infty} k_{Rm}(E) p_m(E) dE - n_A p_B \sum_{m=1}^{M} K_{Rm}^{eq} \int_{E_{0i}}^{\infty} k_{Rm}(E) \frac{\rho_m(E) e^{-\beta E}}{Q_m(\beta)} dE \qquad (2)$$

Over the entire set of energy grains and isomers, Equations (1) and (2) give a set of coupled ordinary differential equations that may be solved using stochastic approaches like kinetic Monte-Carlo[16,17,23] or matrix diagonalization techniques.[24] The advantage of using matrix techniques is the availability of techniques (discussed below) that allow us to solve Eq (1) and (2) directly, and relate their eigenvalues and eigenvectors to temperature and pressure dependent phenomenological rate coefficients of the sorts observed by experimentalists – i.e., the sort of data generally required as input for kinetic mechanisms of combustion and atmospheric chemistry. The disadvantage of using matrix techniques is that there are certain situations (also discussed below) in which numerical instabilities arise, giving unreliable eigenvectors and eigenvalues.[25,26]

In setting up the matrix form of Eq. (1) and (2), the energy grains of the different isomers are concatenated and then indexed using a single index, i, that labels the grains of all of the isomers. The coupled set of differential equations may then be expressed as:

$$\frac{d}{dt}\mathbf{p} = \mathbf{M}\mathbf{p} \qquad (3)$$

where **p** is a vector containing the population densities, $p_m(E)$ and p_B, for the energy grains of all the isomers and the source-term, B. **M,** the transition matrix**,** determines population evolution due to the collisional energy transfer and reaction processes discussed above. **M** is partitioned into blocks: blocks on the diagonal govern collisional energy transfer within isomer *m* as well as reactive loss of that isomer by dissociation or isomerisation. Off-diagonal blocks deal with reactive gain in isomer *m* by inter-conversion from the other isomers or by the association of the reactants, A + B.

Solution of the matrix equation in Eq. (3) provides the time dependence of **p**, and has the form:

$$\mathbf{p} = \mathbf{U}e^{\mathbf{\Lambda}t}\mathbf{U}^{-1}\mathbf{p}(0) \qquad (4)$$

where **p**(0) contains the initial ($t = 0$) conditions for each grain (i.e., p_i(E,0)), **U** is a matrix of eigenvectors obtained from diagonalization of **M**, and **Λ** is a vector of the corresponding eigenvalues. The total number of eigenvalues is equal to the number of grains.

An important constraint on the formulation of the EGME is that of detailed balance, which imposes on the elements **M** the condition $M_{ji}f_i = M_{ij}f_j$, where f_i is the long-time equilibrium population fraction for grain *i*. This condition applies both to collisional energy transfer within a grain and reactive transfer between isomers and the reactants; it has the added practical benefit that the **M** can be symmetrised before diagonalization in order to exploit a number of numerical methods available for the efficient diagonalization of symmetric matrices. The symmetric matrix **S** has elements which are related to the matrix elements of the asymmetric matrix **M** as follows:

$$S_{ij} = M_{ij}\left(\frac{f_i}{f_j}\right)^{1/2} = M_{ji}\left(\frac{f_j}{f_i}\right)^{1/2} = S_{ji} \qquad (5)$$

All transition matrices in MESMER are symmetrised prior to diagonalization.

For a conserved system (i.e., one for which the previously discussed 'infinite sink' approximation is not required, so that the total population density is always unity) with *r* different chemical configurations (isomers, reactants, products), there will be, for low to moderate temperatures, *r* eigenvalues that are substantially smaller in absolute magnitude (i.e., they are less negative) than the other eigenvalues. The first eigenvalue, often referred to as λ_0, is equal to zero, and the corresponding eigenvector gives the equilibrium Boltzmann distribution in each grain.[8,13] For systems that utilize the infinite sink approximation,

diagonalization of **M** does not yield an eigenvalue equal to zero. For both conservative and non-conservative systems, the r eigenvalues are often referred to as the 'chemically significant' eigenvalues (CSEs).[13] Along with their corresponding eigenvectors, they describe the time evolution of the system as it approaches equilibrium. The CSEs are those that correspond to the experimentally observed phenomenological rates measured in typical kinetics experiments, since they describe reaction and inter-conversion between the different molecular configurations on the PES. The remaining eigenvalues – those that are much more negative than the CSEs – correspond to collisional relaxation on very short time scales, and are often referred to as the internal energy relaxation eigenvalues (IEREs).[13]

Key to the EGME approach is the manner in which one calculates: (i) the micro-canonical rate coefficients, $k(E)$, that describe reactive processes which transfer population between reactants, isomers, and products; and (ii) the energy transfer probabilities, $P(E|E')$, which describe how the energy of a reactant molecule is altered as a consequence of inelastic, non-reactive collisions. The transition of a molecule from energy state E to energy state E' is described by a transition probability function, $P(E'|E)$, which is subject to two constraints. It must be normalized – i.e.,

$$\int P(E' \mid E) dE' = 1 \tag{6}$$

and it must obey detailed balance – i.e.,

$$P(E' \mid E) f(E) = P(E \mid E') f(E') \tag{7}$$

where $f(E)$ is the equilibrium (Boltzmann) distribution. Eq. (7) ensures that the EGME gives a thermal Boltzmann distribution in the long-time limit for a conserved system. The transition probability can, in principle, be obtained from quantum or classical scattering calculations, but these are often difficult to perform, and so approximate functional forms with adjustable parameters are typically used. The methods used by MESMER for constructing both microcanonical rate coefficients and collisional energy transfer probabilities are discussed in detail below.

We close this section by mentioning some practical details to be considered in running EGME calculations. The EGME depends on calculating the number of molecular states within each grain. Calculating the grained numbers of states is accomplished by first calculating the numbers of states in so-called "cells", which have an energy width of 1 cm^{-1}. The states within the cells are bundled into grains by summing over the energy width of the grain to give the total number of states per grain. The practical size of the grain should be balanced against two considerations: it should be small enough to permit an adequate level of

microscopic non-equilibrium detail for the system at hand – e.g., it must be smaller than the quantity of energy transferred in a typical inelastic collision event; however, it should not be so small that the matrix diagonalization process is computationally intractable. In principle, it is possible to perform EGME calculations where the grain width is identical to the cell width (1 cm^{-1}); however, for multiwell systems, this level of detail is often unnecessary, and results in an extremely expensive diagonalization process. One generally finds that a grain width of 0.5 – 3 kJ mol^{-1} (40 – 250 cm^{-1}) is a good compromise, and that changes in the grain size do not have a significant effect on the EGME results – i.e., the EGME is converged with respect to grain size. Another practical consideration in running EMGE calculations concerns where to locate the highest energy grain in the system. In general, it should be located high enough in energy that it has no significant population flux over the kinetic timescales of interest. Placing the highest energy grain c.a. $20kT$ above the highest stationary point in the system is generally sufficient.

2. MESMER design

The principal objective of MESMER is to provide a general and flexible program to facilitate ME analysis of unimolecular systems. One of the most significant design goals in writing MESMER has been to provide the flexibility required to perform EGME calculations for stationary point connectivities of arbitrary complexity, far beyond the simple example shown in Scheme 1.

The target users of MESMER were taken to be a broad range of individuals. On the one hand, we anticipate users with a modest awareness of computational methods that wish carry out some form of system modelling to complement, e.g., experimental results. On the other hand, we anticipate more experienced users who are interested in extending a method or algorithm and need to access to the code. The following requirements were thus stipulated at the outset:

1. The application will be open source. Development and extension by other groups is encouraged and the design should allow for easy addition of code.
2. The application will be portable and cross platform, able to run on Windows, OSX, and LINUX.
3. The application will be implemented using standard, off-the-shelf technologies, for which there is copious documentation.

4. The application will be delivered to the end user with build tools.

5. Application data will be represented in a flexible format that can be easily exchanged with other applications.

6. Extended precision methods, based on an existing numerical library, will be accommodated within the application.

7. The application will provide methods and tools to fit experimental data. The nature of the parameter dependence is such that nonlinear methods will be mandatory.

These requirements led to a number of design decisions. First, we decided that the problem is best expressed in terms of objects, with the principal objects being the molecules and reactions that define the system. Second, our desire to use standard and computationally efficient technologies led to the selection of C++ as the principal language for development. Third, given that data representation was identified as a key aspect of MESMER, it has been developed around an Extensible Markup Language (XML) data format, which embraces many of the features of Chemical Markup Language (i.e., CML, see http://www.xml-cml.org/). This means that MESMER data is accessible to a number of other software tools, and can be easily edited, displayed and exchanged. The data are structured in a hierarchy that reflects MESMER's internal object model, with four principal divisions:

1. Species. This division lists all the species (including transition states) that participate in the reaction scheme. Each species includes all the information needed to describe the particular role it plays in the reaction scheme. Species are organized by a molecule manager class that governs their creation and manipulation.

2. Reactions. This division defines the relationships between species by specifying the elementary reactions in which they participate (i.e., the connectivity between isomers, reactants, source terms, or sinks via the relevant transition state). Reactions are organized by a reaction manager class that governs their creation and manipulation.

3. Experimental data. A key task that MESMER has been designed to address is data analysis. This division allows the user to specify conditions of interest and (if available) experimental measurements of a number of kinetic properties. These measurements can be analysed against a proposed model for the system. Variable model parameters may be identified within the 'Species' and 'Reactions' objects, and can be fitted to refine the original model so as to give the best agreement between simulated and experimental data.

4. Control parameters. This division allows the specification of the type of calculation to be performed together with model parameters like the grain width.

The MESMER input format allows for forward and backward compatibility. It also allows extensions to include meta-data that might, e.g., be used to indicate the provenance of experimental data. At execution time the XML input is parsed and creates a set of internal structures reflecting the data in the file. Access to these structures is controlled through a defined API.

MESMER has been developed with a view to exploiting the ever increasing availability of data from *ab initio* quantum chemistry methods, which are increasingly able to predict energies, geometries, and frequencies of stationary points on a reactive system's PES. This presents two separate opportunities. First, calculating transition state properties with quantum chemistry methods is an active research area. There remains a need to evaluate the results of these calculations against experimental data,[22] and MESMER provides a mechanism for achieving this. Second, large-scale system modelling generally involves kinetic schemes with many reactions, and it is often the case that details for many reactions are not available. In combination with *ab initio* methods, MESMER can provide first principles estimates of rate coefficient parameters for use in such models.

It is our hope that MESMER development will not be confined to a small number of developers, but that a group with any particular interest can modify and/or extend the code base in such a way as best meets their needs. To this end the code base has been structured to be easily extendable through the use of plug-in classes. This allows new code to be added to MESMER and invoked through the use of keywords, without altering the code's core architecture. Plug-in class implementations inherit from a set of programmatic interfaces defined as C++ abstract base classes. A number of key components of MESMER utilize plug-in classes in order to formulate the EGME, and these include:

1. Calculation of microcanonical rate coefficients. Plug-in classes presently allow the user access to a number of different methods for calculating $k(E)$ including: (i) RRKM theory, (ii) tunnelling corrected RRKM theory, (iii) the ILT method for calculating $k(E)$s from canonical rate coefficients fit to an Arrhenius expression, and (iv) non-adiabatic microcanonical transition state theory.
2. Calculation of collisional energy transfer probabilities. Plug-in classes presently allow the user access to the exponential down model, which is the most commonly used of energy transfer models.

3. Calculation of rovibrational densities of states (DOS) for isomers, reactants, products, and transition states. Plug-in classes offer a number of different approaches for calculating both external and internal rotational DOS. MESMER can calculate external DOS using both classical and quantum partition functions for linear, spherical, symmetric and asymmetric tops. For internal rotations, MESMER includes a method to calculate the DOS for a quantum mechanical hindered rotor (discussed below).

The general workflow of a typical calculation is shown in scheme 2. Execution begins with parsing the XML input and creating an internal hierarchy representing the data. This hierarchy is further parsed to create a set of objects representing the species and reactions described above. If the user specifies an EGME calculation, the transition matrix is constructed and diagonalized – a process that may occur a number of times depending on the type of calculation MESMER is performing. The output from the diagonalization is then analysed as specified and data are written to the output.

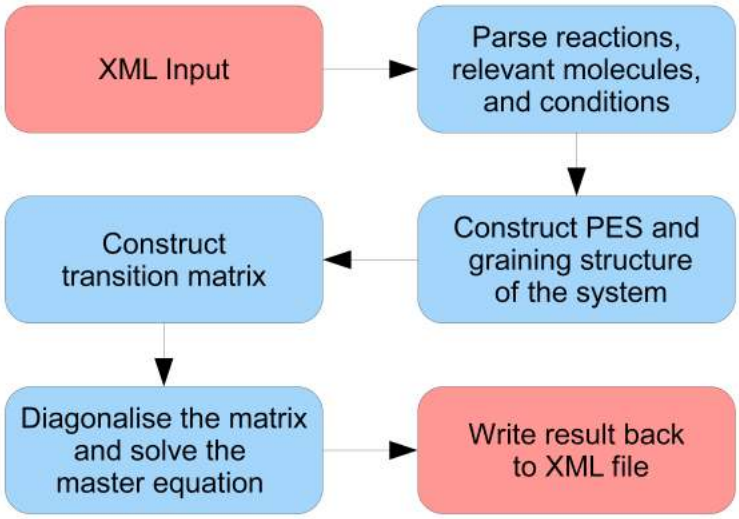

Scheme 2. Workflow for a typical MESMER execution.

While MESMER has primarily been designed to perform EGME calculations, it is important to note that it carries out a number of useful statistical mechanics calculations prior to diagonalizing the EGME transition matrix, **M**. These include the computation of: molecular DOS, canonical partition functions, thermal TST rate coefficients, and RRKM rate coefficients. As none of these tasks require setting up and diagonalizing **M**, we have made it

possible for users to specify that MESMER perform these tasks without solving the full EGME.

MESMER's primary output channel is via the internal data structures created during the initial parsing of the input XML. Calculated data are added to these data structures and all data are persisted at the conclusion of the execution, so that a calculation can be restarted from where it terminated: any datafile can be used as input. There are two other output files: a *.log file which reports the progress of the calculation and logs messages reported during execution, and a *.test file which is used to record more detailed data, often for the purposes of debugging and quality control. Important errors are shown on the console.

At present MESMER is a command line application. However, having the data files in XML format allows them to be edited, visualized and analyzed by external programs. For example, MESMER is currently distributed along with an XSLT stylesheet that transforms the XML to HTML and SVG for displaying input data in Firefox (or another browser). This gives a text display that organizes the data in an easy-to-view and user-friendly form, showing important input properties of the species and reactions, as well as output results. The XSLT is also used to construct diagrams: it shows the reaction potential energy surface as well as plots of output data (e.g., time-dependent species profiles and phenomenological rate coefficients). An example of an energy surface diagram is shown in Figure 1. It provides a quick synopsis of the chemical system, and is especially useful during initial construction or modification of an XML input data file.

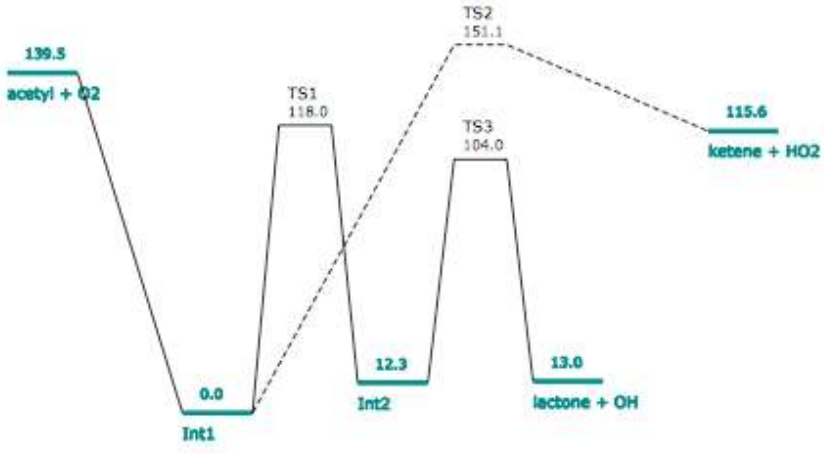

Figure 1. Energy level diagram produced using Firefox from an XSLT transform of an XML datafile.

3. Current implementation details

In this section, we provide an overview of several of the methods and features available in MESMER, paying particular attention to those capabilities that, to our knowledge, are unique to MESMER.

3.1. DOS treatment

Within MESMER, rovibrational DOS are evaluated on the assumption that the rotational DOS are separable from vibrational DOS, which is a good approximation at low energies. There are a number of models for evaluating molecular densities of states, and to accommodate these, MESMER has an abstract interface that allows a new model to be added via a plug-in class. At present MESMER calculates vibrational DOS using the Beyer-Swinehart algorithm in conjunction with a harmonic oscillator approximation.[27] A number of plugin class options are available for calculating the rotational DOS of both external and internal rotors, and are detailed below.

3.1.1. Classical and Quantum Mechanical external rotors

MESMER presently treats external rotors as rigid. This approximation is most reasonable for systems with small numbers of atoms. For larger systems the approximation may be less applicable, as the coupling strength between large-amplitude internal motions and external rotation increases – i.e., the moments of inertia can depend on an internal rotor degree of freedom and there may be significant Coriolis coupling.[28] However, the detailed calculation of these coupling terms is a complex exercise and progress has been largely confined to approaches based on classical mechanics. With a statistical state counting approach, the details of individual states are less important than the number of states within a given energy range, and a rigid rotor approximation often gives a reasonable description of this state distribution. MESMER treats internal and external rotational symmetry using symmetry numbers in the standard way.[29]

MESMER offers a classical and a quantum mechanical (QM) plug-in class with a number of methods for different types of rotors.[27] Details are given in table 1. Each method returns an array which includes the state densities calculated using either a classical

approximation or the exact quantum mechanical state density, g_v. This array is then convolved with the hindered rotor states (if appropriate) and the vibrational DOS.

Type of rotor	MESMER recognition criteria	Rotor type	Classical DOS expression or Quantum energy level expression and degeneracy
not a rotor	No nonzero rotational constants available in the input.	Classical	$\rho(E) = \delta(E)$
2d linear classical rotor	Only one nonzero rotational constant provided in the input	Classical	$\rho(E) = \frac{1}{\sigma B}$
3d classical rotor	Three rotational constants provided in the input	Classical	$\rho(E) = \frac{1}{\sigma}\sqrt{\frac{4E}{ABC}}$
Spherical top	$I_A = I_B = I_C$ ($A = B = C$)	QM	$E_r(J,K)=BJ(J+1)$ $g_{JK} = (2J+1)^2$
Oblate or near oblate symmetric top	$I_A = I_B < I_C$ (A = B > C)	QM	$E_r(J,K)=BJ(J+1)+(C-B)K^2$ J=0,1,2; K=0,±1,±2,…, ±J $g_{JK} = 2J+1$
Prolate or near prolate symmetric top	$I_A < I_B = I_C$ (A > B = C)	QM	$E_r(J,K)=BJ(J+1)+(A-B)K^2$ J=0,1,2;K=0,±1,±2,…, ±J $g_{JK} = 2J+1$
Asymmetric top[30]	$I_A < I_B < I_C$ ($A > B > C$)	QM	$E_r(J)=(A+C)J(J+1)/2+\varepsilon(\kappa)$ $g_{JK} = 2J+1$

Table 1. The methods offered by MESMER for the calculation of rotational DOS.

Approximate provision is also made in these plug-in classes for the contribution from any electronically excited states. If an electronically excited state is present, then an additional manifold of rotation states is added to the DOS array. However, this approximation cannot always be justified – an important example being that of the OH radical, where there is significant coupling between electronic and rotational angular momenta.[31] In order to accommodate these cases, an additional class has been implemented that allows the user to read in their own customized set of rotational-electronic states.

3.1.2. Hindered internal rotors

A number of authors have tackled the issue of hindered internal rotation of a one-dimensional rotor.[32] Some methods have been based on the full analytical solution[33] and others are based on interpolation schemes between harmonic oscillator states and free rotor

states.[34] Here an approached is presented based on the expansion of the one-dimensional hindered rotor Hamiltonian in terms of the free rotor wave functions, which follows closely the development given by Lewis et al.[35] This approach has been implemented within MESMER as it allows consideration of more complex potentials, such as might be obtained from *ab initio* investigations.

The quantum mechanical Hamiltonian for a simple de-coupled one dimensional rotor in the absence of a potential can be expressed as,

$$-\frac{\hbar^2}{2I}\frac{\partial^2}{\partial\theta^2}\psi = E\psi \tag{8}$$

where I is the reduced moment of inertia for internal rotation. The solutions of this equation are well known and can be written as:

$$\psi(\theta) = \frac{1}{\sqrt{2\pi}}e^{ik\theta} \tag{9}$$

where $k = 0,\pm1,\pm2,\cdots$ and the corresponding energies are:

$$E = \frac{\hbar^2 k^2}{2I} \tag{10}$$

These solutions form an orthonormal set such that:

$$\langle k|j\rangle = \frac{1}{2\pi}\int_0^{2\pi} d\theta e^{i(j-k)\theta} = \delta_{jk} \tag{11}$$

which can be used as a basis for forming a representation of the hindered rotor Hamiltonian. For ease of the development, we suppose that the hindering potential can be expressed as (this will be generalized shortly):

$$V(\theta) = \frac{V}{2}(1-\cos n\theta) \tag{12}$$

Hence the hindered rotor Hamiltonian is:

$$\hat{H}\psi = -\frac{\hbar^2}{2I}\frac{\partial^2}{\partial\theta^2}\psi + \frac{V}{2}(1-\cos n\theta)\psi = E\psi \tag{13}$$

which is a specific instance of the Mathieu equation.[36] A representation of this Hamiltonian in the free rotor set can be can be obtained by forming the matrix elements of the Hamiltonian in this basis:

$$\left\langle j\middle|\hat{H}\middle|k\right\rangle = H_{jk} = \left(\frac{\hbar^2 k^2}{2I} + \frac{V}{2}\right)\delta_{jk} - \frac{V}{2}\left\langle j\middle|\cos n\theta\middle|k\right\rangle \tag{14}$$

which reduces to

$$H_{jk} = \left(\frac{\hbar^2 k^2}{2I} + \frac{V}{2} \right) \delta_{jk} - \frac{V}{4} \delta(|k - j| - n) \qquad (15)$$

This expression leads to a banded matrix with the main diagonal populated by free rotor state energies shifted by $V/2$ and an upper and lower diagonal at a distance n from the main diagonal; additional elements associated with $k = 0$ also contribute. As the representation is symmetric it can be diagonalized by standard linear algebra methods.

This approach is variational, so sufficient terms need to be included in the expansion to ensure that the states required by a ME calculation are converged. As the dependence of the main diagonal terms has a k^2 dependency, the number of states that need to be considered is modest, even for a large value of I.

Extension to more complex potentials depends on the symmetry of the potential. If the potential can be represented as a cosine expansion:

$$V(\theta) = \sum_{n=0}^{m} \frac{V_n}{2} \cos n\theta \qquad (16)$$

the corresponding matrix elements are,

$$H_{jk} = \left(\frac{\hbar^2 k^2}{2I} + \frac{V_0}{2} \right) \delta_{jk} + \sum_{n=1}^{m} \frac{V_n}{4} \delta(|k - j| - n) \qquad (17)$$

If the potential is asymmetric then the representation of the potential will include sine terms, i.e.

$$V(\theta) = \sum_{n=0}^{m} \frac{V_n}{2} \cos n\theta + \sum_{l=1}^{m} \frac{V_l}{2} \sin l\theta \qquad (18)$$

For such a potential, the Hamiltonian can be expressed in the same basis and the representation remains hermitian, as required, however, the matrix elements are now complex, with the contribution to a matrix element from the sine terms being

$$\frac{V_l}{2} \langle j | \sin l\theta | k \rangle = \frac{iV_l}{4} [\delta(k - j - l) - \delta(k - j + l)] \qquad (19)$$

As a consequence, the diagonalization of the Hamiltonian matrix must either be done using complex variants of the standard diagonalization routines or the augmented matrix approach.[37] MESMER implements the latter.

An example of the results obtained using this approach is shown in figure 2. This figure plots model potential energy points for the internal rotation about the central C-C bond

of butane, obtained using the DMol module of Materials Studio[38] (B3LYP/DNP). The line running through the points is a Fourier expansion of ten terms that fits the numerical data satisfactorily. Superimposed on this plot are energy levels obtained from the above procedure.

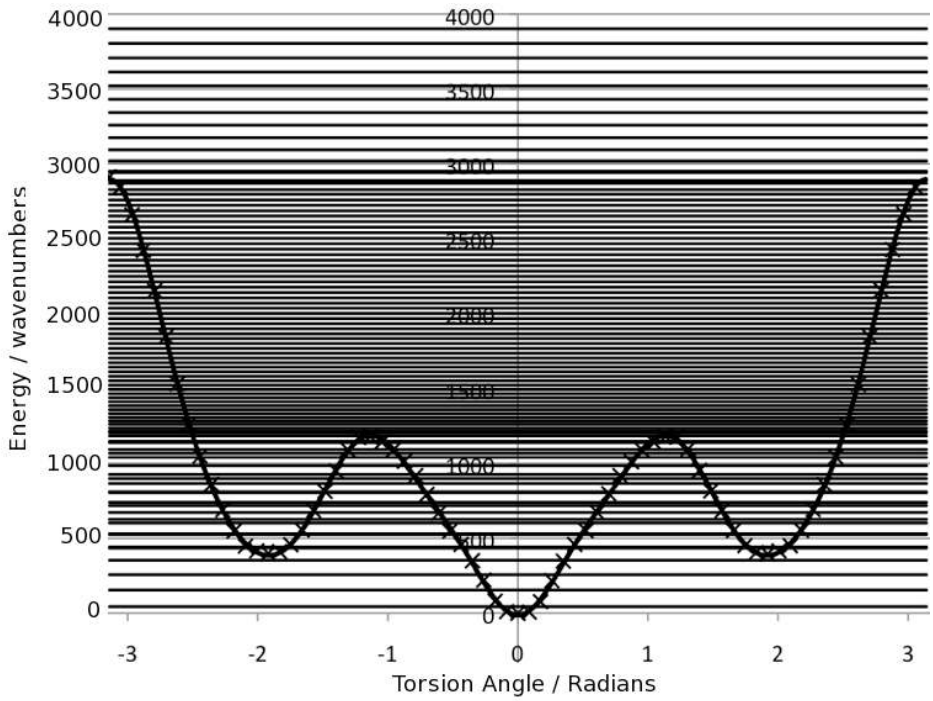

Figure 2. The energy levels (in cm^{-1}) for the hindered internal rotor mode about the central C-C of butane. Points marked × are potential points obtained from ab-initio calculation, the dashed line is a fourier expansion fit to the ab-inito data and the straight, horizontal full lines are the quantum mechanical energy levels.

3.2. Microcanonical rate coefficients

Conversion between reactants, intermediates, and products on a PES such as that shown in Scheme 1 is described within MESMER using microcanonical rate coefficients. In general, these are monotonically increasing functions of a molecule's internal energy, and the different options presently included within MESMER are outlined below.

3.2.1. RRKM

For unimolecular reactions with a well-defined transition state, the most common way of obtaining energy resolved microcanonical rate coefficients for a particular energy grain,

$k(E)$, utilizes RRKM theory, which is a microcanonical formulation of TST. The RRKM expression is:[8]

$$k(E) = \frac{W(E - E_0)}{h\rho(E)} \tag{20}$$

where $W(E - E_0)$ is the rovibrational sum of states (SOS) at the optimized transition state (TS) geometry (excluding the degree of freedom associated with passage through the TS), E_0 is the reaction threshold energy, h is Planck's constant, and $\rho(E)$ is the density of rovibrational states of the reactant. RRKM theory depends on the assumption that the total phase space of a molecule at a particular energy is uniformly populated as the molecule passes from reactant to product through the transition state dividing surface, and the time scale for energy randomization is very short compared with that of reaction, so that a microcanonical ensemble is maintained.[39,40] This is commonly called the ergodicity assumption. The RRKM equation is applicable for transition state dividing surfaces located at a constrained geometry with a well-defined energetic barrier. When the reaction in question is barrierless, a first principles determination of $k(E)$ requires a variational approach – i.e., $k(E)$ is calculated by minimizing $W(E)$ on the PES in question.[41] This approach is not currently available in MESMER; instead we use an approach using inverse Laplace transformation (ILT), which is discussed in the following section.

3.2.2. Unimolecular and association ILT

An alternative to using the RRKM expression for calculating $k(E)$ is to use an ILT. With this technique, the unimolecular microcanonical $k(E)$ is determined from either experimental measurements or theoretical determinations of the canonical high pressure limiting rate coefficient, $k^{\infty}(T)$. So long as the forward $k(T)$s may be cast in the modified Arrhenius form discussed below, then the relationship between $k(E)$s obtained from ILT and the corresponding $k(T)$s is exact – i.e., the ILT method yields a set of forward $k(E)$s which, when multiplied by a Boltzmann distribution and summed, give back the $k(T)$s. For an isomerisation reaction, the microcanonical rate coefficients for the reverse reaction may be straightforwardly determined via detailed balance. The ILT method for obtaining $k(E)$ is particularly well-suited to barrierless reactions, where conventional TST and RRKM theory

are not appropriate because the location of the transition state depends on energy, a situation which is typical of radical-radical associations. In such cases, experimental determinations of $k^{\infty}(T)$ or sophisticated versions of VTST, such as flexible transition state theory (FTST),[42,43] are generally far more accurate. So long as the canonical rate coefficients obtained from either of these approaches can be fitted to an Arrhenius or modified Arrhenius form, then they may be used to calculate accurate $k(E)$s via ILT. MESMER has two implementations of ILT – one for unimolecular dissociation and isomerisation reactions, and one for association reactions. The basis of the ILT methods is that canonical high pressure rate coefficient may be expressed as:

$$k^{\infty}(\beta) = \frac{1}{Q(\beta)} \int_0^{\infty} k(E)\rho(E)\exp(-\beta E)dE \tag{21}$$

where $\rho(E)$ is the reactant rovibrational density of states and $Q(\beta)$ is the corresponding canonical partition function. Letting L denote a Laplace transform and rearranging gives:

$$Q(\beta)k^{\infty}(\beta) = \int_0^{\infty} k(E)\rho(E)\exp(-\beta E)dE = L[k(E)\rho(E)] \tag{22}$$

If $k^{\infty}(\beta)$ can be represented by the modified Arrhenius expression,

$$k^{\infty}(\beta) = A_0\left(\frac{\beta_0}{\beta}\right)^n \exp(-\beta E_a) \tag{23}$$

it follows that:

$$k(E)\rho(E) = A_0\beta_0{}^n L^{-1}\left[Q(\beta)\frac{1}{\beta^n}\exp(-\beta E_a)\right] \tag{24}$$

Further progress can be made by applying the convolution theorem, $L^{-1}\left[Q(\beta)G(\beta)\right] = q \otimes g$, where $\otimes$ denotes convolution, with transform pairs Q, q and G, g. Solving the respective ILTs for use in the convolution theorem gives

$$\begin{aligned} L^{-1}\left[Q(\beta)\right] &= \rho(E) \\ L^{-1}\left[G(\beta)\right] = L^{-1}\left[\frac{1}{\beta^n}\exp(-\beta E_a)\right] &= \frac{(E-E_a)^{n-1}u(E-E_a)}{\Gamma(n)} \end{aligned} \tag{25}$$

where u is the Heavyside step function. Subsequent convolution of these solutions gives:

$$k(E)\rho(E) = \frac{A_0 {\beta_0}^n}{\Gamma(n)} \int_0^E d\tau \rho(E-\tau)(\tau - E_a)^{n-1} u(\tau - E_a) \qquad (26)$$

where τ is a dummy integration variable.

A similar expression can be obtained for the case where the Arrhenius or modified Arrhenius expression provides an accurate representation of the high pressure association rate coefficient. The forward (association) and reverse (dissociation) rate coefficients are related by the equilibrium constant, $K_e(\beta)$, as follows:

$$k_d^\infty(\beta) = K_e(\beta) k_a^\infty(\beta) \qquad (27)$$

where subscript *a* denotes association and subscript *d* dissociation If $k_a^\infty(\beta)$ can be represented using a modified Arrhenius form, then $k(E)$ for dissociation may be obtained using the following ILT equation:

$$k(E)\rho(E) = A_0 {\beta_0}^n L^{-1}\left[Q(\beta) K_e(\beta) \frac{1}{\beta^n} \exp(-\beta E_a) \right] \qquad (28)$$

where the modified Arrhenius parameters now refer to the association rate coefficient. Solving the above equation is complicated by some extra algebra that arises from translational degrees of freedom in the equilibrium constant, but otherwise proceeds as above by exploiting the convolution theorem. The final result (for a reaction of type A + B → C) is:[44]

$$k(E)\rho(E) = \frac{A_0 {\beta_0}^n}{\Gamma(n+1.5)} \left(\frac{2\pi\mu}{h^2} \right)^{3/2} \left(\frac{g_A g_B}{g_C} \right) \int_0^E d\tau \rho_R(E-\tau)(\tau - E_a - \Delta H_0^0)^{n+0.5} u(\tau - E_a - \Delta H_0^0)$$

(29)

where $\rho_R(E)$ is the convolved density of states for the associating pair, ΔH_0^0 is the enthalpy of reaction, μ is the reduced mass of the system and g_X is the spin degeneracy of species X.

3.2.3. Tunneling corrections

Tunnelling and non-classical reflection can be included within the standard RRKM expression by a simple modification of the transition state sum of states as follows:[45]

$$k(E) = \frac{W_{tunn}(E)}{h\rho(E)} \qquad (30)$$

where $W_{tunn}(E)$ is a convolution of the tunnelling transmission probabilities, $P_{\text{tunn}}(E)$, with $\rho^{\text{TS}}(E)$, the transition state DOS – i.e.:

$$W_{\text{tunn}}(E) = \int_{-E_0}^{E-E_0} \rho^{\text{TS}}(E - E_{\text{T}}) P_{\text{tunn}}(E_T) dE_{\text{T}} \qquad (31)$$

where E_0 is the classical barrier height in the direction of the forward reaction, E_T is the energy in the reaction coordinate relative to the top of the energy barrier, E is the total energy, and the zero of energy is chosen to lie at the classical barrier. Presently, MESMER can include tunnelling corrections through an asymmetric Eckart barrier, in which the tunnelling transmission probabilities are calculated as follows:[45]

$$P_{tunn}(E_T) = \frac{\sinh(a)\sinh(b)}{\sinh^2((a+b)/2)\cosh^2(c)}$$
$$a = \frac{4\pi}{h\nu_i}\frac{\sqrt{E_T + E_0}}{(E_0^{-0.5} + V_1^{-0.5})},\ b = \frac{4\pi}{h\nu_i}\frac{\sqrt{E_T + V_1}}{(E_0^{-0.5} + V_1^{-0.5})},\ c = 2\pi\sqrt{\frac{E_0 V_1}{(h\nu_i)^2} - \frac{1}{16}} \qquad (32)$$

where ν_i is the imaginary frequency at the top of the barrier, and V_1 is the classical barrier height with respect to the products.

3.2.4. Non-adiabatic RRKM for spin hopping problem

MESMER also includes an implementation of microcanonical non-adiabatic transition state theory (NA-TST), which is described in detail elsewhere.[46] The manner in which NA-TST is implemented is very similar to the method in which tunnelling corrections are implemented, beginning with the typical RRKM expression, but replacing the sum of states at the TS with the sum of states at the minimum energy crossing point (MECP) between the two diabatic surfaces – i.e.:

$$k(E) = \frac{W_{MECP}(E)}{h\rho(E)} \qquad (33)$$

where $W_{MECP}(E)$ is a convolution of the density of states at the MECP geometry, $\rho_{MECP}(E)$, and the spin forbidden hopping (SH) probabilities, $P_{\text{SH}}(E)$:

$$W_{\text{MECP}}(E) = \int_0^E \rho^{\text{MECP}}(E - E_{\text{H}}) P_{\text{SH}}(E) dE_{\text{H}} \qquad (34)$$

MESMER presently includes a Landau-Zener (LZ) spin hopping model,[47,48] in which:

$$p_{SH}(E_H) = (1+P)(1-P)$$
$$P = \exp\left(\frac{-2\pi H_{12}^2}{h\Delta F}\sqrt{\frac{\mu}{2(E-E_{MECP})}}\right) \quad (35)$$

where $p_{SH}(E_H)$ corresponds to a double passage hopping probability with non-adiabatic transit allowed on both forward and reverse passage through the MECP, H_{12} is the matrix element for coupling between the two surfaces, μ is the reduced mass for movement along the vector orthogonal to the singlet/triplet crossing seam, and ΔF is the relative slope of the two surfaces at the crossing seam. The LZ surface hopping model is best suited to non-adiabatic systems with localized coupling regions and narrowly avoided crossings.

In Eq. (35), the hopping probabilities for energies below the MECP are zero. MESMER includes another method for treating LZ hopping, which additionally allows tunnelling at energies below the MECP using an expression derived from a semiclassical WKB approximation:[49,50]

$$p_{SH}(E_H) = 4\pi^2 H_{12}^2 \exp\left(\frac{-2\mu}{\hbar^2 F\Delta F}\right)^{2/3} Ai^2\left[(E-E_{MECP})\left(\frac{2\mu\Delta F^2}{\hbar^2 F^4}\right)^{1/3}\right] \quad (36)$$

where F is the average of the slopes on the two surfaces at the MECP, and *Ai* denotes the Airy function.

3.3. Phenomenological rate coefficients

Solution of Eq. (3) yields the full microcanonical description of the system time evolution – i.e., for every energy grain in the system. In general, however, this information is more than what is required; one is often interested in the phenomenological rate coefficients for the set of chemical reactions linking the reactants, adduct isomers and products, as well as related quantities such as product yields and branching ratios. It is therefore important to relate the microcanonical information contained in Eq. (3) to the phenomenological quantities of interest. MESMER implements a procedure based upon that described by Bartis and Widom[51] which uses the eigenvectors and eigenvalues obtained from solution of Eq. (3) to provide phenomenological rate coefficients for arbitrary interconnected networks of stationary points.

The mathematical development of the Bartis-Widom technique implemented in MESMER is described by Robertson *et al.*,[10] and so will not be detailed here. Briefly, the basic idea is as follows: for typical atmospheric and combustion systems, the phenomenologi-

cal time evolution for an arbitrarily interconnected kinetic system of molecular species is typically described using a coupled set of differential equations, similar in form to those of Eq. (3), with the difference that the population of each species is represented by a single term in the population vector rather than a set of energy grains. Assuming that n species make up the kinetic scheme, the coupled set of differential equations may be written using an $n \times n$ rate coefficient matrix **K** representing n coupled first order or pseudo first order differential equations:

$$\frac{d}{dt}\mathbf{c} = \mathbf{K}\mathbf{c} \tag{37}$$

where the matrix element K_{ab} is the rate coefficient $k_{b\to a}(T,P)$ for all possible reactions and **c** is a vector of species concentrations. Diagonalization of this rate matrix yields a solution in terms of n eigenvalues and n eigenvectors. The principle difference between **M** and **K** is that the matrix elements of the latter do not include an explicit description of collisional relaxation, which occurs on timescales much shorter than those which characterize phenomenological kinetics.

The Bartis-Widom method exploits the separation between the internal energy relaxation eigenvalues (IEREs) and chemically significant eigenvalues (CSEs): assuming that the CSEs obtained from the diagonalization of **M** (which explicitly include collisional relaxation) are identical to those which could be obtained from diagonalization of **K**, then the $n \times n$ phenomenological rate matrix **K** may be reconstructed from the CSEs using simple matrix algebra. The Bartis-Widom analysis is a useful technique because it provides a global description of the time dependent kinetics in terms of $n \times n$ rate coefficients, and in many cases, the phenomenological rate coefficient is the quantity of interest to be obtained from a ME calculation. However, the Bartis-Widom analysis relies on the separation between CSEs and IEREs. If these are not well separated (practically speaking, by more than an order of magnitude), the system cannot be represented by a set of first order rate equations linking the concentrations of the n species in the vector **c.** This means that the rate coefficients provided by the Bartis-Widom analysis are unreliable and MESMER will print a warning. In such cases, and so long as numerical precision is not an issue, the user may rely on the species profiles to analyse the system kinetics, since these do not require separation between CSEs and IEREs. When there is good separation between the CSEs and the IEREs (i.e., at least an order of magnitude), then the species profiles obtained from the full EGME are effectively

identical to the species profiles which can be obtained from the Bartis-Widom phenomenological rate coefficients.

3.4. Addressing numerical precision

Because MESMER uses numerical matrix techniques to formulate and solve the ME, it is not immune to numerical precision problems.[25,26,52] The difficulty arises in diagonalization of the transition matrix where, for certain conditions, the ratio of the largest to the smallest eigenvalue exceeds machine precision. In general, this can occur for deep wells, low temperatures, and low pressures. While the origin of these effects and when they occur is reasonably well understood, solutions to these problems are less well developed. MESMER includes a few different ways of dealing with numerical precision problems when they arise.

3.4.1. Increased precision libraries

The contracted basis set and reservoir state approaches, both of which are described below, are elegant ways of manipulating the mathematical formulation of the ME to delay the onset of numerical problems; however, we have also incorporated within MESMER a brute force technique for carrying out the diagonalization using significantly increased numerical precision available in a set of cross-platform libraries.[53] By specifying input file keywords, users can select the precision of the arithmetic (double, double-double or quad-double) utilized in the diagonalization. The maximum precision currently possible, approximately octuple, corresponds to a mantissa of 59 decimal places, but requires a significantly higher computational overhead.

3.4.2. Reservoir state methods

The basis of the reservoir state (RS) approach (which has a number of similarities to the previously proposed methods[4,19,54]) is the notion that grains which are low in energy with respect to the top of an energy barrier exist in a steady state distribution that is not significantly perturbed by events at the threshold. As such, these grains can be lumped

together and treated as a single reservoir that acts as both a sink and a source. Figure 3 shows a schematic representation of the reservoir state.

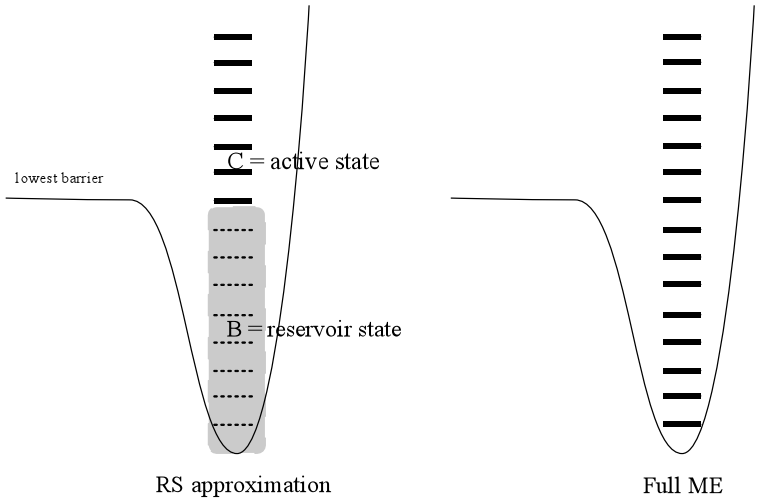

Figure 3 – Schematic representation of the RS approximation and the full master equation simulations for a one-well system with a bimolecular source term. The RS approximation lumps a set of grains into a single grain (the reservoir) and assumes that a Boltzmann distribution is maintained within the reservoir over the timescales of interest.

The RS approximation is good when the transition probabilities for activating collisions between the reservoir grains and the higher energy grains are small – i.e., at low temperatures or when the system involves deep wells, both of which are common circumstances in which the full EGME suffers problems with numerical precision. The RS approximation exploits the fact that the most interesting non-equilibrium kinetic behaviour modelled by the ME takes place in the energy space above any particular barrier. Consequently, so long as a reservoir state is separated from the barrier by an energy larger than that typically transferred during collision events, it does not significantly affect what happens in the region of the barrier. In general, the RS approximation performs better at low temperatures than high temperatures. Conveniently, this is precisely the regime in which the RS is required because solution of the full EGME rarely leads to numerical instabilities at high temperatures.

MESMER allows the user to choose the energy space spanned by a particular RS, as its optimum size often depends on the particular details of the system under investigation. The mathematical details of the RS approximation are discussed in detail in the Supplementary Information (SI), along with a number of numerical tests carried out using the MESMER implementation. Our tests have shown that MESMER's implementation of the RS approximation improves numerical stability in regimes which are problematic for the full

EGME. Where comparisons are possible, the RS method gives results in excellent agreement with the full EGME. For some systems, the RS approximation results in computational speedups of nearly an order of magnitude.[52]

3.4.3. Contracted basis method

The mathematic details of the contracted basis method are outlined in Appendix A. The practical objective of this method is similar to that of the RS method: to accurately represent a full EGME system using a reduced matrix and thus reduce the computational expense of the diagonalization. This approach is closely related to that proposed by Venkatesh and co-workers,[55,56] who expressed the ME in a basis of analytic functions rather than δ-functions; however, it differs insofar as the basis functions are derived from a grained solution to a single well master equation. The present approach is also closely related to the perturbation approach described by Snider[57] and elements of it have been used more recently by Miller and co-workers in their analysis of detailed balance.[22] Some preliminary results for an approximate model of the isomerisation between the primary and secondary pentyl radicals are presented in the SI.

3.5. Collisional energy transfer models

The most common model for calculating collisional energy transition probabilities is the so-called exponential down model, and this is what is presently implemented within MESMER. The exponential down model, which assumes that the energy transfer probability depends only on the internal energy of the molecule, and not on its collisional history or its configuration, calculates collisional energy transition probabilities as:[9,13,58]

$$P(E \leftarrow E') = C(E')\exp\left(-\frac{E'-E}{\langle \Delta E \rangle_d}\right) \tag{38}$$

where $E' > E$, $C(E')$ is a normalization constant, and $\langle \Delta E \rangle_d$ is the average energy transferred per collision in a downward direction. The transition probabilities for energy transfer in the upward direction may be obtained via detailed balance. The exponential down model was proposed on the basis of results from scattering theory,[59,60] and reflects the common sense

notion that collisions which transfer large amounts of energy are less probable than those that transfer small amounts of energy.[9] Other models with different transition probability distributions have been proposed, such as Gaussian models[27] and double exponential models.[13] It has often been noted that classical trajectory simulations as well as experimental data suggest that the exponential down model is perhaps not the most accurate for describing collisional transition probabilities, and that models with longer tails are more accurate.[13,58,61-64]

Nevertheless, most published EGME studies utilize the single exponential down model.[5] This is partially because other functions (e.g., double exponential models) feature more parameters, and systematic techniques for assigning parameter values have yet to be established. Additionally, given the extensive use of the single exponential down model in the literature, a set of typical $\langle \Delta E \rangle_d$ values has emerged. For example, at room temperature He bath gas tends to have $\langle \Delta E \rangle_d$ values from ~50-300 cm^{-1},[26,65-70] while O_2 and N_2 bath gases tend to have slightly higher $\langle \Delta E \rangle_d$ values of ~250-500 cm^{-1}.[67,69,71] In general, $\langle \Delta E \rangle_d$ is left as a variable parameter determined by fitting to experimental data, within the limits given above, and it usually shows a slight positive temperature dependence in one dimensional ME analyses. The origin of the temperature dependence is not entirely clear, although it has been suggested that it may relate to rotational relaxation,[72] an observation which is compatible with the fact that classical trajectory calculations have identified the dependence of $\langle \Delta E \rangle_d$ on the angular momentum of the target molecule.[20] Experimentally, higher temperatures correspond to higher angular momentum states, and in the one-dimensional ME, this may be manifest as an effective increase in $\langle \Delta E \rangle_d$.[72]

3.6. Data fitting methods

As discussed above, the analysis of experimental data is often an important objective for MESMER. For example, one might want to fit experimental data in order to obtain a reaction threshold or high pressure Arrhenius parameters. It is generally the case that the calculated rate coefficients have a non-linear dependence on these parameters, in which case it is normal to optimize the χ^2 merit function using an algorithm based on the Levenberg-Marquardt approach. However, such an algorithm requires a knowledge of the derivatives of

the rate coefficients with respect to the parameters. The difficulty with this is that the rate coefficients are derived from eigenvalues of the matrix **M**, which are calculated numerically. In general, there is no direct analytic relationship between the rate coefficients and the parameters on which they depend, so that analytic derivatives cannot be calculated.

This leaves the option of numerical derivatives, despite the fact that they often involve a large computational expense with an increase in the number of fit parameters. The expense arises because derivatives for a particular parameter requires calculation of χ^2 for (at least) two other points in parameter space, resulting in several diagonalizations of **M** at each pressure and temperature point in the experimental set. Hence it is advantageous to invoke as few diagonalizations as possible in minimizing χ^2.

MESMER offers two approaches to the optimization of χ^2: the Powell conjugate direction method and a Levenberg-Marquardt approach based on numerical derivatives.[37] The Powell conjugate direction method requires line searches to be performed in the chosen parameter space and these are done using golden section searches. The directions of the line searches are initially taken as the set of mutually perpendicular unit vectors of the parameter space, but these search directions are updated as the individual line searches are completed in accordance with Powell's algorithm. The Levenberg-Marquardt implementation follows a standard pattern with the minor alteration that limits can be placed on the range of values a parameter may take during a search. Our experience to date suggests that the Levenberg-Marquardt algorithm, despite initial heavy costs, is the most efficient method.

4. Examples

4.1. MESMER test examples

During the implementation of MESMER, a number of tests were developed in order to monitor the impact of code changes and provide a test suite for future developments. These test systems are supplied with the MESMER distribution and are based on a number of previous studies, most of which are relevant to combustion and atmospheric chemistry. Included in these tests are:

(1) Simple unimolecular dissociation – i.e., the decomposition of the iso-propyl radical to propene and a hydrogen atom, which includes the quantum mechanical treatment of hindered internal rotors described above;[73]

(2) Isomerization reactions of the n-pentyl radical;[10]

(3) The reaction of the acetyl radical with excess oxygen, an example of a two-well system. It features a source term, a tunnelling treatment, and fitting to experimental data using a minimum χ^2 criterion.[67] The association of CH_3CO + O_2 has been shown experimentally to give OH at low pressures because of isomerisation and subsequent dissociation of the initially formed peroxy radical. This type of chemistry, which involves so-called "formally direct" kinetics, is important in reactions of peroxy radicals in combustion.[74]

(4) The reaction of the H radical with SO_2,[75] which features a bimolecular source term and makes use of extended precision libraries for matrix diagonalization;

(5) The reaction of OH with NO, which features a bimolecular source term, and an example of how to use MESMER to perform a so-called "thermodynamic data" calculation. The results of this calculation give $\Delta H(T)$, $\Delta S(T)$, and $\Delta G(T)$ for OH, NO, and HNO_2 at a range of temperatures.

4.2. Atmospheric chemistry

MESMER has so far been applied to a number of chemical kinetic systems relevant to both terrestrial and extra-planetary atmospheres, including:

(1) The pressure and temperature dependence of the reaction of OH with acetylene, which includes a bimolecular source term and an ILT treatment of the association process;[69]

(2) The atmospheric kinetic sequence that follows association between the benzene-OH adduct and O_2, which involves a bimolecular source term with multiple association channels;[76]

(3) The kinetics between $O_2(^1\Delta_g)$ + Ca, which utilizes increased precision arithmetic, non-adiabatic spin-hopping kinetics, and ILT treatments to describe both association and dissociation processes.[77]

(4) An examination of the kinetics between $^1CH_2$ and acetylene, which implements a reservoir state approximation and matrix diagonalization using increased numeri-

cal precision and three reservoir states.[52,78] This reaction produces the C_3H_3 radical, which can act as a route to benzene and lead to subsequent haze formation in Titan's atmosphere.

(5) The atmospheric abstraction and addition kinetics of OH + polybrominated diphenyl ethers (PBDEs).[79]

4.3. Organic chemistry

In addition to the aforementioned examples, we have successfully applied MESMER to understand experimentally observed kinetics and product yields in solution phase synthetic chemistry. To our knowledge, these studies represent the first time that master equation treatments have been extended to solution phase systems. So far, the systems we have investigated include:

(1) The hydroboration of propene to give OH substituted Markovinikov and anti-Markovnikov products.[3] This system implements a source term and an isolated binary collision treatment of solvent-solute relaxation. The EGME quantitatively reproduces the experimentally observed product ratios observed at different temperatures, and suggests the reaction occurs in a regime where chemical reaction timescales compete with collisional relaxation timescales.

(2) [1,5] Hydrogen migration in chemically activated cyclopentadiene.[2] Again, using an isolated binary collision treatment of solvent-solute relaxation, the EGME was able to provide a good description of the experimentally observed hydrogen migration yield arising from a chemically activated cyclopentadienyl radical. The results suggest that the reaction occurs in a regime where chemical reaction timescales compete with collisional relaxation timescales.

5. Conclusions, outlook, future development

The goal of the MESMER application is to facilitate the analysis and interpretation of kinetic rate data for systems whose potential energy surface consists of a number of stationary points, and where system-bath energy transfer affects kinetic outcomes. In the limit of very high pressures, MESMER gives rate coefficients which are identical to those obtained from thermal TST, while in the limit of very low pressures, MESMER gives rate coefficients which

are identical to those obtained from RRKM theory. MESMER is particularly well suited to analyzing kinetics in intermediate pressure regimes, where a great deal of chemistry in nature occurs. Alongside increasingly accurate thermodynamics data, continuing developments in electronic structure theory, improved fundamental understanding of energy transfer within gas and condensed phases, and expanding databases of reliable experimental data, we envision that tools like MESMER will eventually enable reliable and routine prediction of non-equilibrium kinetics in arbitrary systems.

With this vision in mind, MESMER has been built to provide a user-friendly, open-source, object oriented framework with a number of key design principles that we hope will facilitate open-source development: (1) the MESMER object model allows the natural definition (and extension) of molecular species and the reactions in which they participate, and this is reflected in MESMER's flexible, XML based, I/O facility; (2) through the device of plugin classes, it should be relatively straightforward for a number of workers to extend the code and contribute to the development of MESMER, and (3) MESMER includes the provision of facilities to analyse and fit data, which will enable us to construct a database for analysis and fitting.

The development of MESMER is ongoing and potential future work includes:

- The development of a graphical user interface (GUI). While the use of an XML based data format is key to the interoperability of MESMER with other applications, and there are a number of XML editors available, the input of data would be greatly assisted by a user interface that supported the MESMER data specification.
- A wide range of databases are available that contain information pertinent to a MEMSER calculation, e.g. thermochemical and *ab initio* properties databases such as those made available by NIST, or through active thermochemical tables.[80] It would be of enormous benefit to the research community if a means of interfacing these databases with MESMER could be established.
- Central to almost all MESMER calculations is the diagonalization of a matrix, and the performance of MESMER depends on the efficiency of this diagonalization. In the case of data fitting, diagonalization must be performed a large number of times for different conditions and parameter values. This permits an "embarrassingly parallel" implementation of MESMER built on libraries such as MPI or openMP. In addition, we are carrying our further investigation of efficient mathematical formulations tailored to the specifics of the problem at hand (e.g. basis contraction and reservoir states).

- Once a reaction system has been analysed, reporting a set of rate coefficients and/or eigenvalues at specific temperatures and pressures is usually not the most convenient form for use in macroscopic models. Hence we are exploring methods to efficiently represent output data in more useful forms.
- Our recent work in applying EGME approaches to solution phase organic chemistry opens up the possibility of extending MESMER to treat the chemistry that occurs in a range of condensed phase and interfacial systems. These will likely require research and development of more accurate energy transfer models that go beyond the simple exponential down model.

Acknowledgements

This work was made possible through the help of several people not included as authors, in particular Robin Shannon, Dr. Mark Blitz, Dr. Nicholas Green, Dr. Kevin Hughes, Dr. David Waller, and Professor Paul Seakins. Much of the MESMER development was carried out under the auspices of grants from the EPSRC and NERC.

References

1. Truhlar, D. G.; Garrett, B. C.; Klippenstein, S. J. J Phys Chem 1996, 100(31), 12771-12800.
2. Goldman, L. M.; Glowacki, D. R.; Carpenter, B. K. J Am Chem Soc 2011, 133(14), 5312-5318.
3. Glowacki, D. R.; Liang, C. H.; Marsden, S. P.; Harvey, J. N.; Pilling, M. J. J Am Chem Soc 2010, 132(39), 13621-13623.
4. Allen, J. W.; Goldsmith, C. F.; Green, W. H. PCCP Phys Chem Chem Phys 2012, 14(3), 1131-1155.
5. Golden, D. M.; Barker, J. R. Combust Flame 2011, 158(4), 602-617.
6. Barker, J. R.; Golden, D. M. Chemical Reviews (Washington, DC, United States) 2003, 103(12), 4577-4591.
7. Glowacki, D. R.; Pilling, M. J. ChemPhysChem 2010, 11(18), 3836-3843.
8. Holbrook, K. A.; Pilling, M. J.; Robertson, S. H. Unimolecular Reactions; John Wiley & Sons: Chichester, 1996.
9. Pilling, M. J.; Robertson, S. H. Annu Rev Phys Chem 2003, 54, 245-275.
10. Robertson, S. H.; Pilling, M. J.; Jitariu, L. C.; Hillier, I. H. Phys Chem Chem Phys 2007, 9(31), 4085-4097.
11. Miller, J. A.; Pilling, M. J.; Troe, J. Proc Combust Inst 2005, 30(Pt. 1), 43-88.
12. Miller, J. A.; Klippenstein, S. J.; Raffy, C. J Phys Chem A 2002, 106(19), 4904-4913.
13. Miller, J. A.; Klippenstein, S. J. J Phys Chem A 2006, 110(36), 10528-10544.
14. Klippenstein, S. J.; Miller, J. A. J Phys Chem A 2002, 106(40), 9267-9277.
15. Miller, J. A.; Klippenstein, S. J. J Phys Chem A 2003, 107(15), 2680-2692.
16. Gillespie, D. T. In Annu Rev Phys Chem; Annual Reviews: Palo Alto, 2007, p 35-55.
17. Barker, J. R. Int J Chem Kinet 2001, 33(4), 232-245.
18. Robertson, S. H.; Pilling, M. J.; Gates, K. E.; Smith, S. C. J Comput Chem 1997, 18(8), 1004-1010.
19. Green, N. J. B.; Bhatti, Z. A. PCCP 2007, 9(31), 4275-4290.
20. Barker, J. R.; Weston, R. E. J Phys Chem A 2010, 114(39), 10619-10633.
21. Smith, S. C.; Gilbert, R. G. Int J Chem Kinet 1988, 20(4), 307-329.
22. Miller, J. A.; Klippenstein, S. J.; Robertson, S. H.; Pilling, M. J.; Green, N. J. B. PCCP Phys Chem Chem Phys 2009, 11(8), 1128-1137.
23. Vereecken, L.; Huyberechts, G.; Peeters, J. Journal of Chemical Physics 1997, 106(16), 6564-6573.
24. Frankcombe, T. J.; Smith, S. C. J Theor Comput Chem 2003, 2(2), 179-191.
25. Frankcombe, T. J.; Smith, S. C. Theor Chem Acc 2009, 124(5-6), 303-317.
26. Gannon, K. L.; Glowacki, D. R.; Blitz, M. A.; Hughes, K. J.; Pilling, M. J.; Seakins, P. W. J Phys Chem A 2007, 111(29), 6679-6692.
27. Gilbert, R. G.; Smith, S. C. Theory of Unimolecular and Recombination Reactions; Blackwell Scientific Publications: Oxford, 1990.
28. Gang, J.; Pilling, M. J.; Robertson, S. H. Chem Phys 1998, 231(2-3), 183-192.
29. Fernandez-Ramos, A.; Ellingson, B. A.; Meana-Paneda, R.; Marques, J. M. C.; Truhlar, D. G. Theor Chem Acc 2007, 118(4), 813-826.
30. King, G. W.; Hainer, R. M.; Cross, P. C. Journal of Chemical Physics 1943, 11(1), 27-42.
31. Hougen, J. T. NBS Monograph 1970, 115.
32. Chuang, Y. Y.; Truhlar, D. G. Journal of Chemical Physics 2000, 112(3), 1221-1228.
33. Nielsen, H. H. Phys Rev 1932, 40(3), 0445-0456.

34. Barker, J. R.; Shovlin, C. N. Chemical Physics Letters 2004, 383(1-2), 203-207.
35. Lewis, J. D.; Malloy, T. B.; Chao, T. H.; Laane, J. J Mol Struct 1972, 12(3), 427-&.
36. Abramowitz, M.; Stegun, I. A. Handbook of Mathematical Functions: New York, 1972.
37. Press, W. H.; Teukolsky, S. A.; Vetterling, W. T.; Flannery, B. P. Numerical Recipes in C++; Cambridge University Press: Cambridge, 2002.
38. Accelyrs-Software. San Diego, CA, 2011.
39. Lourderaj, U.; Hase, W. L. J Phys Chem A 2009, 113(11), 2236-2253.
40. Baer, T.; Hase, W. L. Unimolecular reaction dynamics: theory and experiments; Oxford University Press: New York, 1996.
41. Klippenstein, S. J.; Green, N. J. B. In Comprehensive Chemical Kinetics; Elsevier, 2003, p 55-103.
42. Georgievskii, Y.; Klippenstein, S. J. Journal of Chemical Physics 2003, 118(12), 5442-5455.
43. Georgievskii, Y.; Klippenstein, S. J. J Phys Chem A 2003, 107(46), 9776-9781.
44. Davies, J. W.; Green, N. J. B.; Pilling, M. J. Chemical Physics Letters 1986, 126(3-4), 373-379.
45. Miller, W. H. J Am Chem Soc 1979, 101(23), 6810-6814.
46. Harvey, J. N. PCCP Phys Chem Chem Phys 2007, 9(3), 331-343.
47. Jasper, A. W.; Zhu, C. Y.; Nangia, S.; Truhlar, D. G. Faraday Discuss 2004, 127, 1-22.
48. Nikitin, E. E. Annu Rev Phys Chem 1999, 50, 1-21.
49. Harvey, J. N.; Aschi, M. Faraday Discuss 2003, 124, 129-143.
50. Delos, J. B.; Thorson, W. R. Physical Review A 1972, 6(2), 728-&.
51. Bartis, J. T.; Widom, B. Journal of Chemical Physics 1974, 60(9), 3474-3482.
52. Gannon, K. L.; Blitz, M. A.; Liang, C. H.; Pilling, M. J.; Seakins, P. W.; Glowacki, D. R. J Phys Chem A 2010, 114(35), 9413-9424.
53. Hida, Y.; Li, X. S.; Bailey, D. H. Arithmetic 2000, 15.
54. Schranz, H. W.; Nordholm, S. Chem Phys 1983, 74(3), 365-381.
55. Venkatesh, P. K.; Dean, A. M.; Cohen, M. H.; Carr, R. W. Journal of Chemical Physics 1999, 111(18), 8313-8329.
56. Venkatesh, P. K.; Dean, A. M.; Cohen, M. H.; Carr, R. W. Journal of Chemical Physics 1997, 107(21), 8904-8916.
57. Snider, N. S. Journal of Chemical Physics 1965, 42(2), 548-&.
58. Barker, J. R. Int J Chem Kinet 2009, 41(12), 748-763.
59. Jackson, J. M.; Mott, N. F. Proc R soc Lond Ser A-Contain Pap Math Phys Character 1932, 137(833), 703-717.
60. Penner, A. P.; Forst, W. Journal of Chemical Physics 1977, 67(11), 5296-5307.
61. Lenzer, T.; Luther, K.; Reihs, K.; Symonds, A. C. Journal of Chemical Physics 2000, 112(9), 4090-4110.
62. Hold, U.; Lenzer, T.; Luther, K.; Reihs, K.; Symonds, A. C. Journal of Chemical Physics 2000, 112(9), 4076-4089.
63. Hold, U.; Lenzer, T.; Luther, K.; Symonds, A. C. Journal of Chemical Physics 2003, 119(21), 11192-11211.
64. Jasper, A. W.; Miller, J. A. J Phys Chem A 2011, 115(24), 6438-6455.
65. Golden, D. M.; Barker, J. R.; Lohr, L. L. J Phys Chem A 2003, 107(50), 11057-11071.
66. Miller, J. A.; Senosiain, J. P.; Klippenstein, S. J.; Georgievskii, Y. J Phys Chem A 2008, 112(39), 9429-9438.
67. Carr, S. A.; Glowacki, D. R.; Liang, C. H.; Baeza-Romero, M. T.; Blitz, M. A.; Pilling, M. J.; Seakins, P. W. J Phys Chem A 2011, 115(6), 1069-1085.

68. Zador, J.; Klippenstein, S. J.; Miller, J. A. J Phys Chem A 2011, 115(36), 10218-10225.
69. McKee, K. W.; Blitz, M. A.; Cleary, P. A.; Glowacki, D. R.; Pilling, M. J.; Seakins, P. W.; Wang, L. J Phys Chem A 2007, 111(19), 4043-4055.
70. Goldsmith, C. F.; Green, W. H.; Klippenstein, S. J. J Phys Chem A 2012, 116(13), 3325-3346.
71. Goldsmith, C. F.; Klippenstein, S. J.; Green, W. H. Proceedings of the Combustion Institute 2011, 33, 273-282.
72. Miller, J. A. Faraday Discuss 2001, 119(Combustion Chemistry: Elementary Reactions to Macroscopic Processes), 461-475.
73. Seakins, P. W.; Robertson, S. H.; Pilling, M. J.; Slagle, I. R.; Gmurczyk, G. W.; Bencsura, A.; Gutman, D.; Tsang, W. J Phys Chem 1993, 97(17), 4450-4458.
74. Clifford, E. P.; Farrell, J. T.; DeSain, J. D.; Taatjes, C. A. J Phys Chem A 2000, 104(49), 11549-11560.
75. Blitz, M. A.; Hughes, K. J.; Pilling, M. J.; Robertson, S. H. J Phys Chem A 2006, 110(9), 2996-3009.
76. Glowacki, D. R.; Wang, L. M.; Pilling, M. J. J Phys Chem A 2009, 113(18), 5385-5396.
77. Plane, J. M. C.; Whalley, C. L.; Soriano, L.; Goddard, A.; Harvey, J. N.; Glowacki, D. R.; Viggiano, A. A. Journal of Chemical Physics in press.
78. Gannon, K. L.; Blitz, M. A.; Liang, C. H.; Pilling, M. J.; Seakins, P. W.; Glowacki, D. R.; Harvey, J. N. Faraday Discuss 2010, 147, 173-188.
79. Zhou, J.; Chen, J. W.; Liang, C. H.; Xie, Q.; Wang, Y. N.; Zhang, S. Y.; Qiao, X. L.; Li, X. H. Environ Sci Technol 2011, 45(11), 4839-4845.
80. Ruscic, B.; Pinzon, R. E.; Morton, M. L.; Srinivasan, N. K.; Su, M. C.; Sutherland, J. W.; Michael, J. V. J Phys Chem A 2006, 110(21), 6592-6601.
81. Szabo, A.; Ostlund, N. S. Modern Quantum Chemistry; Dover: New York, 1996.
82. Bramley, M. J.; Handy, N. C. Journal of Chemical Physics 1993, 98(2), 1378-1397.

Appendix A

As discussed above, the ME can be solved by expressing the operator **M** in a convenient basis to give a matrix representation which is then diagonalized to obtain the eigenvalues and eigenvectors from which rate coefficients can be derived. Typically, the solution begins by lumping molecular states together to form discrete grains with average properties such as energy, densities of states, etc. The EGME representation uses these grains as basis in which to express **M**, effectively expressing molecular properties in a set of δ-functions. While other basis sets have been proposed,[54-56] this basis remains popular on account of its convenience and ease of interpretation. It does, however, lead to large matrices which are costly to diagonalize. If repeated evaluation is required (as in a fitting exercise) the computational expense can be very large. The problem is exacerbated because the expense of the diagonalization typically goes as N^3, where N is the dimension of the matrix representation. Thus, more wells leads to more grains, and a correspondingly more expensive calculation.

As has been described above and elsewhere[8] the EGME representation of **M** tends to have a block diagonal structure. The diagonal blocks represent reactive loss and energy transfer (excitation and de-excitation) within a species. Sparse off-diagonal blocks represent conversion between species. It is this block diagonal structure that is exploited in this section, borrowing from the methods of basis contraction that are used to solve a number of problems in quantum chemistry.[81,82] The object is to find an alternative basis set with which to represent the ME operator **M**, which leads to a smaller matrix that accurately describes the system.

To begin, consider the case of simple unimolecular dissociation reaction with one well and one channel. An EGME representation of the operator, $\mathbf{M}$, can be formed and is often written as:

$$\mathbf{M} = \omega(\mathbf{P} - \mathbf{I}) - \mathbf{K} \qquad \text{(A1)}$$

where ω is the collision frequency, $\mathbf{P}$ is a matrix representation of the collisional transition probability and $\mathbf{K}$ is a diagonal matrix of microcanonical rate coefficients averaged over each grain. By construction, $\mathbf{P} - \mathbf{I}$ is conservative and so can be symmetrized:

$$\mathbf{S} = \mathbf{F}(\mathbf{P} - \mathbf{I})\mathbf{F}^{-1} \qquad \text{(A2)}$$

where $\mathbf{F}$ is a diagonal matrix whose elements are the square root of the Boltzmann distribution for the well. The matrix $\mathbf{S}$ can be diagonalized to yield a set of eigenvalues and vectors:

$$\mathbf{SU} = \mathbf{U\Lambda} \qquad \text{(A3)}$$

Since $\mathbf{F}$ is a similarity transform, the eigenvalues of $\mathbf{S}$ will be the same as those of $\mathbf{P-I}$ and, from conservation, it follows that there must be at least one eigenvalue, λ_0, that is zero. The corresponding eigenvector, $\mathbf{u}_0$, has elements which are the square root of the Boltzmann distribution for the well, and are identical to the diagonal elements of $\mathbf{F}$.

The matrix $\mathbf{M}$ can also be symmetrized by $\mathbf{F}$:

$$\mathbf{M'} = \mathbf{FMF}^{-1} \tag{A4}$$

and can be diagonalized in this form to obtain the rate coefficient as the modulus of the eigenvalue of smallest magnitude. Alternatively, we can recast $\mathbf{M'}$ in terms of the eigenvectors of $\mathbf{S}$ – i.e., we can use these eigenvectors as a basis set in which to express $\mathbf{M'}$**:**

$$\mathbf{M''} = \mathbf{UM'U}^{-1} = \omega\Lambda - \mathbf{UKU}^{-1} = \omega\Lambda - \mathbf{K'} \tag{A5}$$

The basis set $\mathbf{U}$ is complete and because $\mathbf{M''}$ is a similarity transform of $\mathbf{M'}$, it has the same eigenvalues. The elements of $\mathbf{K'}$ can be written using Dirac notation:

$$K'_{ij} = \langle i|\mathbf{K}|j\rangle \tag{A6}$$

where $|i\rangle$ is the *i*th eigenvector of $\mathbf{S}$. One element that can be written down easily is K'_{00}:

$$K'_{ij} = \langle 0|\mathbf{K}|0\rangle = k_\infty \tag{A7}$$

which is the limiting high pressure rate coefficient. The Matrix $\mathbf{M''}$ thus has the appearance,

$$\mathbf{M''} = \begin{pmatrix} -k_\infty & -K'_{01} & \cdots \\ -K'_{10} & \omega\Lambda_1 - K'_{11} & \cdots \\ \vdots & \vdots & \ddots \end{pmatrix}' \tag{A8}$$

It is interesting to consider the case where we confine the representation of $\mathbf{M''}$ to just the first two eigenvectors in this basis, i.e. forming the reduced representation:

$$\mathbf{M''} = \begin{pmatrix} -k_\infty & -K'_{01} \\ -K'_{01} & \omega\Lambda_1 - K'_{11} \end{pmatrix} \tag{A9}$$

(where the symmetry of $\mathbf{K'}$ has been invoked**).** This representation can be diagonalized analytically. However if $k_\infty K'_{11} \approx \left(K'_{01}\right)^2$ (a constraint that might be applied to ensure that the rate coefficient has the correct limiting behaviour with respect to ω), then:

$$\left(k_\infty + \omega\lambda_1 - K'_{11}\right)^2 >> k_\infty(K'_{11} - \omega\lambda_1) - \left(K'_{01}\right)^2 \tag{A10}$$

and a perturbation type analysis can be applied. This gives an eigenvalue whose smallest magnitude is

$$\varepsilon \approx \frac{k_\infty(K'_{11} - \omega\lambda_1) - \left(K'_{01}\right)^2}{k_\infty + \omega\lambda_1 - K'_{11}} \tag{A11}$$

Applying the above constraint, assuming that $K'_{11} < k_\infty$ and noting that λ_1 is negative, it can be seen that the Lindemann type form is recovered.

This analysis of a single well system does not produce any immediate benefits in terms of computational speed, as the diagonalization of the **S** matrix takes the same time as that of the **M** matrix, given that they are of the same size (though as k_∞, K'_{01} and K'_{11} are independent of pressure this may lead to methods for the rapid calculation of complete fall-off curves). Benefits begin to accrue when larger, multi-well systems are investigated. This can be seen by considering a simple isomerisation reaction (e.g. between species A and B), for which the transition matrix after symmetrisation can be written:

$$\mathbf{M}' = \begin{pmatrix} \omega_A \mathbf{S}_A - \mathbf{K}_A & \overline{\mathbf{K}} \\ \overline{\mathbf{K}}^T & \omega_B \mathbf{S}_B - \mathbf{K}_B \end{pmatrix} \tag{A12}$$

This transition matrix can be analysed in a similar way as the single well example above. To construct a useful basis set consider the case when there is no reaction i.e. $\mathbf{K}_A = \mathbf{K}_B = \overline{\mathbf{K}} = \mathbf{0}$. In these circumstances the transition matrix is block diagonal with each block describing the energy transfer evolution of each isomer. The transition matrix can be diagonalized by diagonalizing each block independently, yielding two sets of eigenvalues and eigenvectors. The two sets of eigenvectors are not only mutually orthogonal amongst themselves but they are also orthogonal with respect to each other. This orthogonality between sets occurs because the eigenvectors, while being of the same dimension as the transition matrix, only have non-zero elements in those components that correspond to one or other isomer. Hence, the overall matrix, $\mathbf{U}$, is block diagonal:

$$\mathbf{U} = \begin{pmatrix} \mathbf{U}_A & \mathbf{0} \\ \mathbf{0}^T & \mathbf{U}_B \end{pmatrix} \tag{A13}$$

Each block has a zero eigenvalue, which corresponds to equilibrium in each isomer, and a corresponding eigenvector describing a Boltzmann distribution in each isomer.

With this basis set, the analogous similarity transform to that given above is,

$$\mathbf{M}'' = \begin{pmatrix} \mathbf{U}_A & \mathbf{0} \\ \mathbf{0}^T & \mathbf{U}_B \end{pmatrix} \begin{pmatrix} \omega_A \mathbf{S}_A - \mathbf{K}_A & \overline{\mathbf{K}} \\ \overline{\mathbf{K}}^T & \omega_B \mathbf{S}_B - \mathbf{K}_B \end{pmatrix} \begin{pmatrix} \mathbf{U}_A & \mathbf{0} \\ \mathbf{0}^T & \mathbf{U}_B \end{pmatrix}^T \tag{A14}$$

which on multiplication gives,

$$\mathbf{M}'' = \begin{pmatrix} \omega_A \Lambda_A - \mathbf{U}_A \mathbf{K}_A \mathbf{U}_A^T & \mathbf{U}_A \overline{\mathbf{K}} \mathbf{U}_B^T \\ \mathbf{U}_B \overline{\mathbf{K}}^T \mathbf{U}_A^T & \omega_B \Lambda_B - \mathbf{U}_B \mathbf{K}_B \mathbf{U}_B^T \end{pmatrix} \tag{A15}$$

As it stands, there remains little to be gained in terms of performance by using this basis transformation; however, as suggested by the manipulations above, the hope is that a

representation using a reduced set can be constructed which will yield the chemically significant eigenvalues at a lower cost. For example, suppose an isomerisation system consists of two isomers of approximately the same well depth which can each be represented by N grains: the cost of diagonalizing each energy transfer transition matrix will be of the order of $2N^3$. Using N/2 basis functions from each set to construct a reduced representation of the overall transition matrix and diagonalizing adds a further cost of N^3, giving an overall cost of $3N^3$; whereas the cost of diagonalizing the original representation will be approximately $(2N)^3 \sim 8N^3$.

As a trivial example, consider the case where the reduced basis set is formed from the first eigenvector associated with each isomer, i.e. the square root of the Boltzmann distribution of each isomer. In this basis, $\mathbf{M}''$ may be written as

$$\mathbf{M}'' = \begin{pmatrix} -k_\infty^A & -K_{00}^{AB} \\ -K_{00}^{AB} & -k_\infty^B \end{pmatrix} \tag{A16}$$

for which the eigenvalues are given by,

$$\varepsilon^2 + \left(k_\infty^A + k_\infty^B\right)\varepsilon + k_\infty^A k_\infty^B - \left(K_{00}^{AB}\right)^2 = 0 \tag{A17}$$

It follows from detailed balance that

$$k_\infty^A k_\infty^B = \left(K_{00}^{AB}\right)^2 \tag{A18}$$

Thus,

$$\varepsilon = 0, -\left(k_\infty^A + k_\infty^B\right) \tag{A19}$$

as obtained from a phenomenological analysis in the high pressure limit.

A similar analysis can be applied to linearized association reactions (i.e., bimolecular source terms), which after symmetrisation can be represented as

$$\mathbf{M}' = \begin{pmatrix} \omega_A \mathbf{S}_A - \mathbf{K}_A & \varphi \\ \varphi^T & -k_b \end{pmatrix} \tag{A20}$$

where k_b is the overall association rate coefficient and the vector φ is the symmetrised exchange between source and well. Following the same procedure as above leads to a basis set,

$$\mathbf{U} = \begin{pmatrix} \mathbf{U}_A & \mathbf{0} \\ \mathbf{0}^T & 1 \end{pmatrix} \tag{A21}$$

Apply this transform to $\mathbf{M}'$ gives,

$$\mathbf{M}'' = \begin{pmatrix} \omega_A \varphi_A - \mathbf{U}_A \mathbf{K}_A \mathbf{U}_A^T & \mathbf{U}_A \varphi \\ \varphi^T \mathbf{U}_A^T & -k_b \end{pmatrix} \tag{A22}$$

The reduced basis set approach outlined in this appendix has been implemented in MESMER and an initial assessment made by modelling a simple isomerisation system based on the inter-conversion of primary and secondary pentyl radicals. Results and timings are discussed in the supplementary information. We expect that the basis set contraction method may have uses in extended precision calculations as well as in so-called “two dimensional ME models”, which account for angular momentum conservation. These 2d master equation treatments generally result in very large matrices, and contraction schemes may offer a useful size reduction.

Supplementary Information

MESMER: An open-source **M**aster **E**quation **S**olver for **M**ulti-**E**nergy well **R**eactions

David R. Glowacki, Chi-Hsiu Liang, Christopher Morley, Michael J. Pilling, and Struan H. Robertson

Contracted basis set approach

The contracted basis set approach outlined in the associated paper has been tested by modelling a simple isomerisation system based on the inter-conversion of primary and secondary pentyl radicals, which has been described previously.[1] External rotors were treated classically and all internal modes where treated as harmonic oscillators. Bath gas parameters for Argon were used to define the collision frequency. A grain size of 100 cm^{-1} was used and the maximum energy was set as 24300 cm^{-1}. Two types of calculation where run: a full ME calculation using the standard δ–function basis set, which gave an overall matrix size of 561, and a contracted basis set calculation using a basis derived from the first 100 eigenvectors of each isomer, giving an overall matrix of dimension 200. For this system there are two chemically significant eigenvalues, one of which is zero and is associated with the equilibrium distribution.

Table 1 shows the value of the second chemically significant eigenvalue (the value responsible for determining the relaxation of the system on chemically significant time scales) for temperatures of 600 K and 1000 K and a range of bath gas concentrations. As can be seen, agreement between the two methods is best at high concentrations, and tends to degrade as the concentration decreases, with the situation being worse at lower temperatures. This is not entirely surprising because the contracted basis has a bias toward the equilibrium distribution and more basis functions may be required for lower pressures. Further investigation of this point is in progress. On a standard desktop machine running windows 7, the calculation takes 20 s using a δ-function basis set, and 13 s using a contracted basis set.

Temperature/K	Concentration/ molec/cm^3	δ-function basis set	Contracted basis set	Ratio
600	10^{12}	-1.77	-6.50	3.68
600	10^{13}	-1.55×10	-3.58×10	2.31
600	10^{14}	-1.23×10^{2}	-1.39×10^{2}	1.13
600	10^{15}	-8.53×10^{2}	-8.66×10^{2}	1.02
600	10^{16}	-4.82×10^{3}	-4.83×10^{3}	1.00
600	10^{17}	-2.05×10^{4}	-2.05×10^{4}	1.00
600	10^{18}	-5.88×10^{4}	-5.88×10^{4}	1.00
600	10^{19}	-1.03×10^{5}	-1.03×10^{5}	1.00
600	10^{20}	-1.23×10^{5}	-1.23×10^{5}	1.00
1000	10^{12}	-1.82	-2.57	1.41
1000	10^{13}	-1.82×10	-2.38×10	1.31
1000	10^{14}	-1.82×10^{2}	-1.95×10^{2}	1.07
1000	10^{15}	-1.82×10^{3}	-1.83×10^{3}	1.01
1000	10^{16}	-1.82×10^{4}	-1.82×10^{4}	1.00
1000	10^{17}	-1.82×10^{5}	-1.82×10^{5}	1.00
1000	10^{18}	-1.81×10^{6}	-1.81×10^{6}	1.00
1000	10^{19}	-1.19×10^{7}	-1.19×10^{7}	1.00
1000	10^{20}	-3.90×10^{7}	-3.90×10^{7}	1.00

Table 1. The second chemically significant eigenvalue for the pentyl radical isomerisation model as calculated by standard and contracted basis set methods.

Reservoir state approach

Formulation

To describe the reservoir state approximation, we begin with the following reaction scheme, schematized in Figure 3 of the main text:

$$B \rightleftharpoons C \qquad \text{(R1)}$$

where the forward rate constant, k_a, represents the rate constant for activation from the reservoir state, *B*, into the active state, *C*. The backward rate constant, k_d, represents the rate constant for deactivation from the active state, *C*, into the reservoir state, *B*. At equilibrium, the forward and reverse rates are equal, i.e.:

$$k_a x_B = k_d x_C \qquad \text{(E1)}$$

where x_B and x_C are the equilibrium fractions of *B* and *C*. Both k_a and k_d are canonical rates of reaction and so depend on temperature, but each is related to their corresponding microcanonical rate constants $k(E)$. The canonical deactivation rate, k_d, is related to the microcanonical deactivation rate coefficients, $k_d(E)$, through the following relation:

$$k_d = \sum_E k_d(E)\frac{f(E)}{Q_C} \qquad \text{(E2)}$$

where $f(E) = \rho(E)\exp(-\beta E)$ and $Q_C = \sum_E f(E)$. The $k_d(E)$s correspond to the energy dependent rates at which species in grains within the non-reservoir region, C, are deactivated

into the reservoir state B. To get the $k_d(E)$s for deactivation from a grain in C into the reservoir B, we sum the normalized downward transition probabilities, $P(i \mid E)$, for deactivation of a particular grain in *C* into *every possible grain* in B. If B spans the energy range from E_0 to E_t and C spans the energy range from E_{t+1} to E_∞, then the $k_d(E)$s for deactivation of a grain *E* in C to the reservoir state B are calculated as follows:

$$k_d(E) = \omega \sum_{i=E_0}^{E_t} P(i \mid E) \qquad \text{(E3)}$$

where ω is the collision frequency. Substituting (E2) into (E1), we obtain:

$$k_a x_B = \sum_E k_d(E) \frac{f(E)}{Q_C} x_C \qquad \text{(E4)}$$

where the term $f(E)x_C / Q_C$ represents the equilibrium fraction in grain *E* of the active state C and the $k_d(E)$s are calculated according to (E3).

The asymmetric ME transition matrix, **M**, requires microcanonical rate coefficients that describe both forward and reverse transition from the reservoir B to the grains in C. In practice though, we only need to calculate the $k_d(E)$s because the symmetrised ME matrix, **S**, needs to have reservoir row and column vectors that are identical by detailed balance, as discussed in the main text.

$$S_{ij} = M_{ij} \left(\frac{f_j}{f_i} \right)^{1/2} \qquad \text{(E4)}$$

Let us say that an active state, C, has *N* grains, so that the row and column that correspond to transitions with the reservoir state have index *N*+1. Recognizing that the $M_{N+1 \leftarrow j}$ matrix elements are equivalent to $k_d(E)$, then f_j is equivalent to $f(E)x_C / Q_C$ and f_{N+1} is equivalent to x_B. Plugging these into (E4) and letting $i \equiv N+1$, we obtain matrix elements of **S** which describe transitions between the reservoir state and grains with energies spanning 1 to *N*:

$$S_{N+1,E} = S_{E,N+1} = k_d(E) \left(\frac{f(E)}{Q_C} x_C \cdot \frac{1}{x_B} \right)^{1/2} \qquad \text{(E5)}$$

The final matrix element, $S_{N+1,N+1}$, is simply k_a, the canonical loss rate coefficient describing population loss from the reservoir state to all the activated grains in C. Writing the (R1) equilibrium constant, *K* as

$$K = \frac{k_a}{k_d} = \frac{x_C}{x_B} \qquad \text{(E6)}$$

then k_a may be obtained by rearranging (E6):

$$k_a = K \cdot k_d = S_{N+1,N+1} \qquad \text{(E7)}$$

Results

The reservoir state approximation has two advantages compared to the full energy grained master equation (EGME): (1) it results in a smaller transition matrix, making the diagonalization procedure more efficient, and (2) it often shows numerical stability over a wider range of pressures, temperatures, and well depths. We have tested the reservoir state approximation on one-well, two-well, and three well systems to check its performance with respect to the full EGME. Molecular parameters and test files for each of these systems are available online (http://sourceforge.net/projects/mesmer/). In what follows, we describe reservoir tests run on three different systems. While these studies give good insight into the applicability of the RS method, it is important to emphasize that reliable application of the RS method requires a careful comparison with results obtained from solution of the EGME over a range of conditions.

OH + HCCH: one-well reservoir state

The OH + HCCH system, shown in Figure 1, has been described previously.[2] OH + HCCH were modelled using a bimolecular source term, and passage over TS1_a was treated as an irreversible sink. In the reservoir state tests described below, we set the top of the reservoir to 2 kJ mol^{-1} below the association barrier.

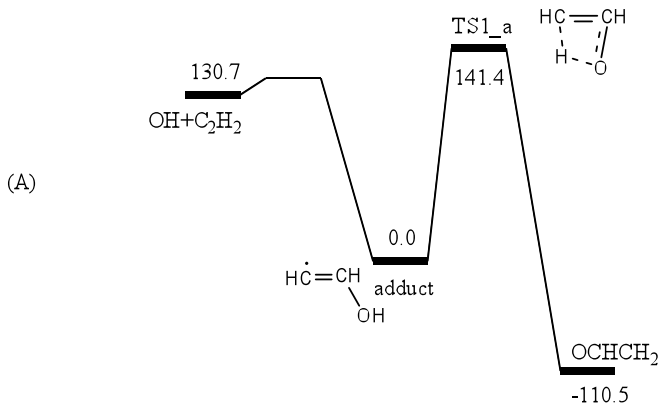

Figure 1 – stationary points for OH + HCCH association. Energies shown are in kJ mol^{-1}

Figure 2 shows comparisons between the RS approximation and the full ME over a range of temperatures and pressures. As shown in the plots, the rate coefficients and yields

obtained using the MESMER RS approximation are in excellent agreement with results obtained using the full EGME over a broad pressure and temperature range. Disagreement occurs at high temperatures (e.g., 1200 K), where it is a less good approximation to assume that the molecular population is thermalized and resides in the reservoir state.

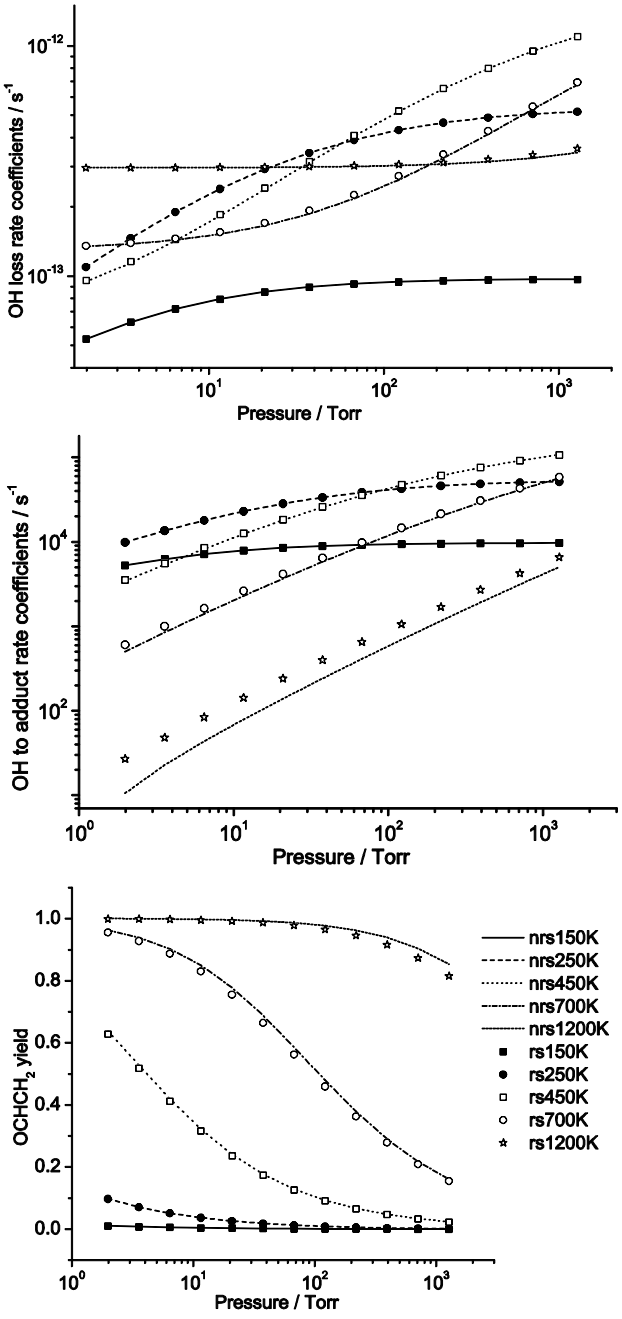

Figure 2: Comparison of OH + HCCH results obtained using the full EGME (denoted nrs) and the reservoir state approximation (denoted rs) over a range of pressures and temperatures for: (top panel) the total OH loss rate coefficient; (middle panel) the association rate coefficient, and (bottom panel) the yield via TS1_a. All results were obtained using double precision arithmetic except those at 150K, which used double-double precision.

Acetyl + O_2: one and two-well reservoir states

The acetyl + O_2 reaction, shown in Figure 3, has been described previously.[3]

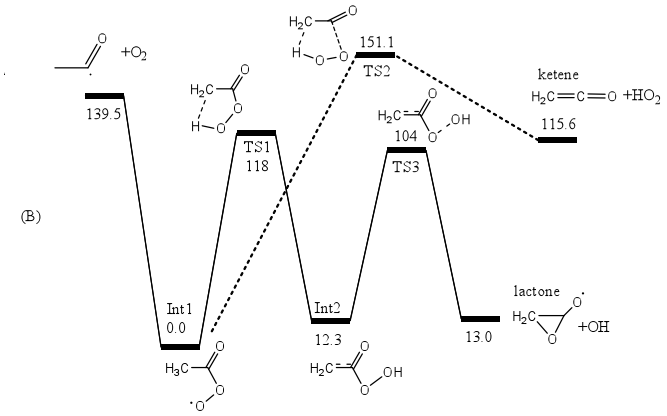

Figure 3: stationary points for O_2 + acetyl association. Energies shown are in kJ mol^{-1}

In our reservoir state tests of this system, we examined a simple one-well model with no dissociation channels as well as the full two-well model which included two dissociation channels. Again, the reservoir size was set to 2 kJ mol^{-1} lower than the lowest barrier for each well, while the grain size was set to 100 cm^{-1}. The bath gas was Helium.

In the one-well test, we examined the acetyl + O_2 association process using only a single well and a bimolecular source term. Figure 4 shows the results of our one-well tests on the total acetyl loss rate coefficient. Again, we note that the agreement of the RS approximation is less satisfactory at high temperatures (e.g., 700 K) and low pressures, where it becomes a less good approximation to assume that the population is thermalized and resides in the reservoir state. Compared to the full EGME, the RS approximation gives association rate coefficients which have improved numerical stability at temperatures lower than 125K.

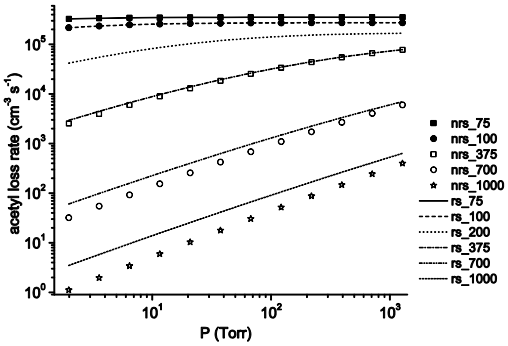

Figure 4: Comparison of one-well O_2 + acetyl results obtained using the full EGME (nrs) and the reservoir state approximation (rs) over a range of pressures and temperatures for the total acetyl loss rate coefficient

In the two-well tests, the full scheme in Figure 3 was included, with reservoir states in both wells, and reaction via TS1 and TS3 treated as infinite sinks. Figure 5 shows the excellent agreement between the full EGME and the RS results in this system. Furthermore, whereas the full EGME showed numerical instabilities below 100 K for the acetyl→Int1, rate coefficient, the reservoir state results were stable.

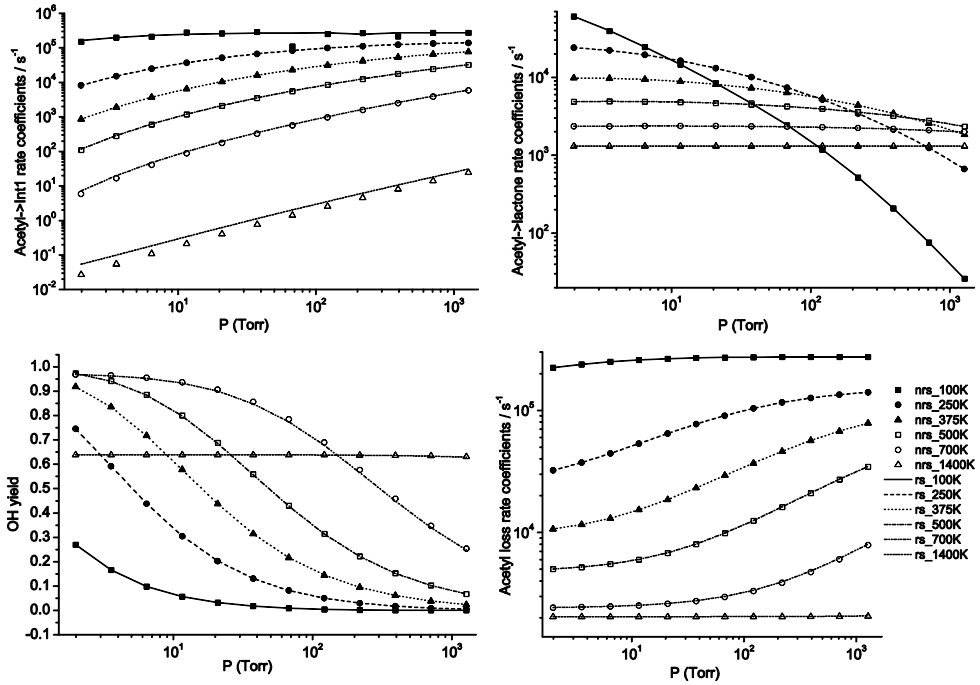

Figure 5: Comparison of two-well O_2 + acetyl results obtained using the full EGME (nrs) and the reservoir state approximation (rs) over a range of pressures and temperatures for: (top left panel) the acetyl→Int1 rate coefficient; (top right panel) the acetyl→lactone rate coefficient; (bottom right panel) the total acetyl loss rate coefficient, and (bottom left panel) the OH yield via TS3.

$^1CH_2 + C_2H_2$: three-well reservoir states

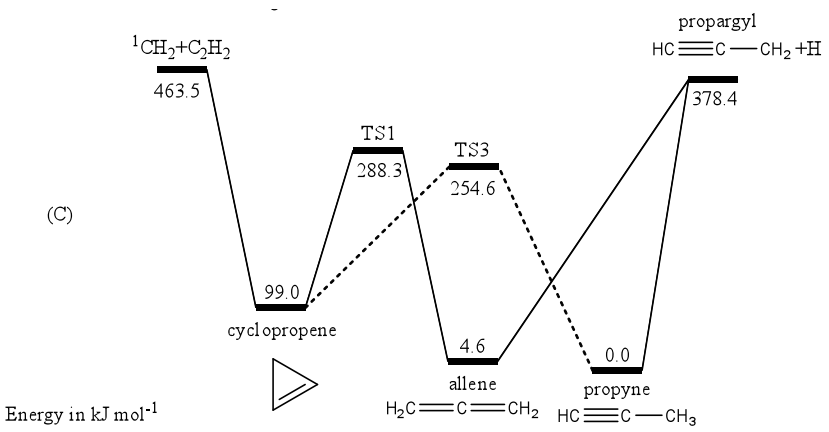

Figure 6: stationary points for $^1CH_2 + C_2H_2$. Energies shown are in kJ mol^{-1}

The $^1CH_2 + C_2H_2$ association reaction, shown in Figure 6, has been described previously[4] and modelled as a three well system with a bimolecular source term and an irreversible sink to propargyl + H. The very large well depths of this system resulted in significant numerical instability in the full EGME, making this system a good target for the RS approach (with a RS located in each of the three wells). Comparisons between the RS approach and the full EGME were run for temperatures from 200 – 1400K and pressures from 1 – 1.5 $\times 10^6$ Torr. Most calculations were done in quad-double, the highest precision available in MESMER. 200 – 400 K results are shown in Figure 7. In general the graphs show good agreement between the RS approximation and the full EGME. Even at higher temperatures (1000 – 1400K, which are not shown in the graphs), the isomers are thermalized at moderate pressures on account of the deep wells, and the RS approximation performs well.

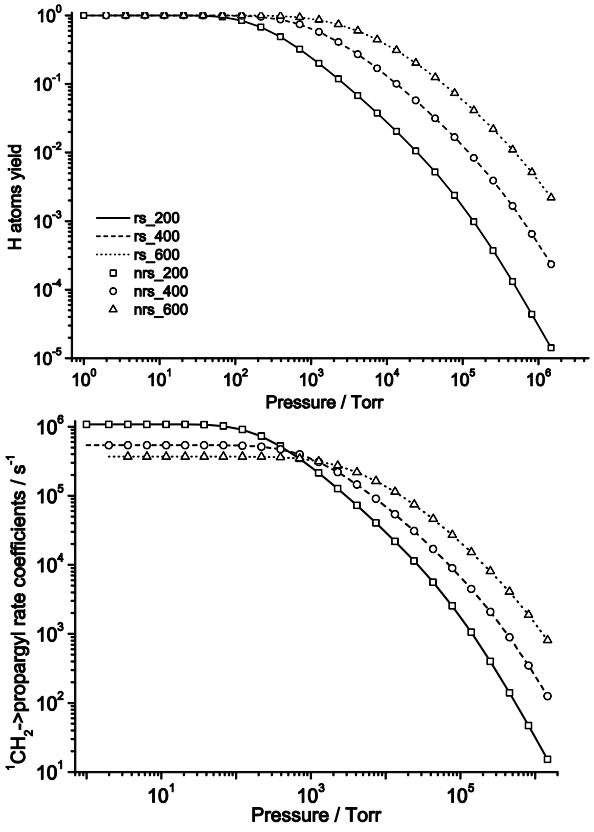

Figure 7 – Comparison of three-well $^1CH_2 + C_2H_2$ results obtained using the full EGME (nrs) and the reservoir state approximation (rs) over a range of pressures and temperatures for: (top panel) the propargyl + OH yield and (bottom panel) the $^1CH_2 \rightarrow$propargyl + H rate coefficient.

In general, we found that rate coefficients obtained using the Bartis-Widom method (discussed in the main text and shown in Figure 7) performed much better for this system than the species profiles. This is because the Bartis-Widom method relies only on a few

eigenvalues (the chemically significant eigenvalues, or CSEs), and the separation of CSEs from the internal energy relaxation eigenvalues (IEREs) is better under low temperature conditions. Figure 8 shows species profiles obtained using both the RS approximation and full EGME over 600 - 800 K (1 Torr). In general, the RS results show improved stability compared to results obtained from solution of the full EGME.

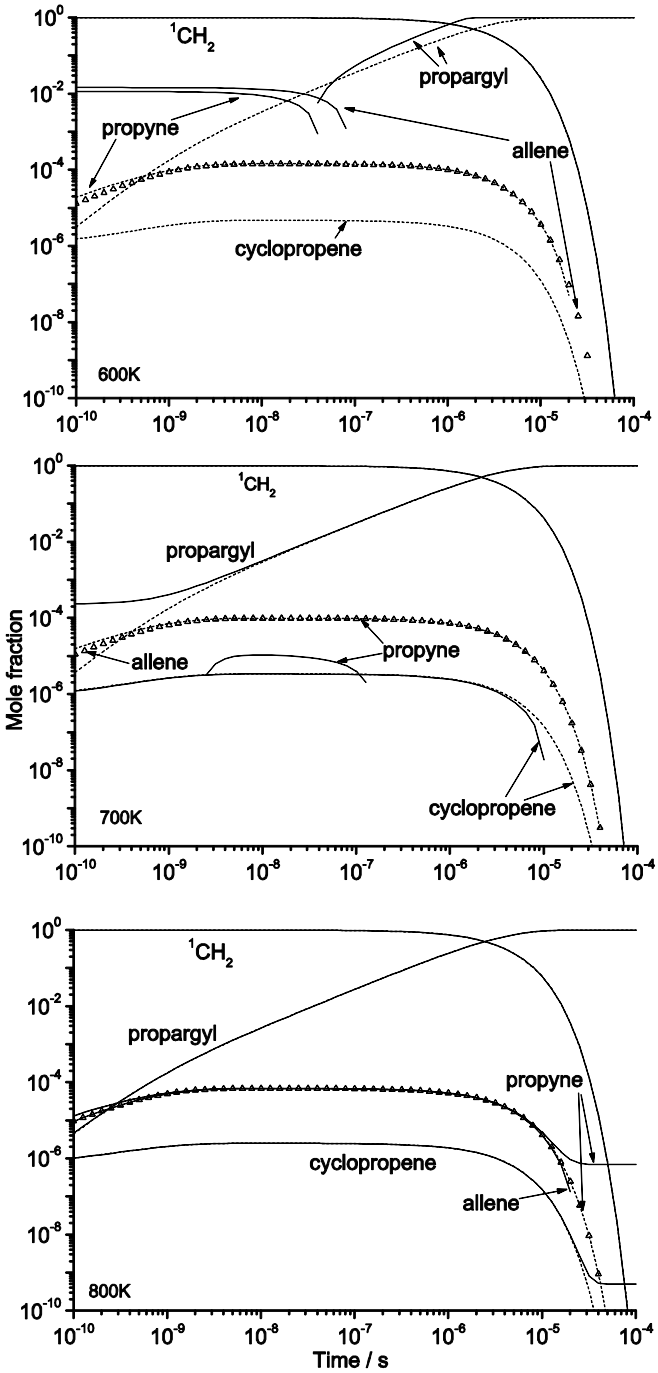

Figure 8: Species profiles obtained from simulations of the $^1CH_2+C_2H_2$ reaction at a pressure of 1Torr and 600 (top), 700 (middle), and 800 K (bottom). The dashed lines show the RS approximation profiles, and the solid

lines show the data obtained from solution of the full EGME. The allene population from the RS approximation is marked by unfilled triangles to avoid ambiguity.

Finally we note that, compared to the time required to solve the full EGME for this system, the RS approximation introduces a factor of eight computational speed-up owing to reduction in size of the matrix to be diagonalized.

6. References

1. Robertson, S. H.; Pilling, M. J.; Jitariu, L. C.; Hillier, I. H. Phys Chem Chem Phys 2007, 9(31), 4085-4097.
2. McKee, K. W.; Blitz, M. A.; Cleary, P. A.; Glowacki, D. R.; Pilling, M. J.; Seakins, P. W.; Wang, L. J Phys Chem A 2007, 111(19), 4043-4055.
3. Carr, S. A.; Glowacki, D. R.; Liang, C. H.; Baeza-Romero, M. T.; Blitz, M. A.; Pilling, M. J.; Seakins, P. W. J Phys Chem A 2011, 115(6), 1069-1085.
4. Gannon, K. L.; Blitz, M. A.; Liang, C. H.; Pilling, M. J.; Seakins, P. W.; Glowacki, D. R. J Phys Chem A 2010, 114(35), 9413-9424.